DIFFERENTIAL CODE SHIFT REFERENCE IMPULSE RADIO ULTRA-WIDEBAND TRANSCEIVER: BIT ERROR RATE TESTS AND PERFORMANCE ASSESSMENTS

by

Bhargava Sahukar

Submitted in partial fulfilment of the requirements
for the degree of Master of Applied Science

at

Dalhousie University
Halifax, Nova Scotia
October 2015

Dedication

This thesis is dedicated to my parents

TABLE OF CONTENTS

LIST OF TABLES.....vi

LIST OF FIGURES.....vii

ABSTRACT…….……x

LIST OF ABBREVIATIONS AND SYMBOLS USED.....xi

ACKNOWLEDGEMENTS.....xiv

CHPATER 1 INTRODUCTION…….……1

1.1 Impulse Radio Background..……...1

1.2 Research Motivation……....2

1.3 Outline of the Thesis…….……...4

CHAPTER 2 UWB DEFINITIONS AND SIGNALING METHODS……..…...…….....6

2.1 FCC Regulations……..6

2.2 UWB Signaling Schemes…….…11

2.2.1 MB Orthogonal Frequency Division Multiplexing……..11

2.2.2 Impulse Radio Ultra-wideband…..…….……..……12

2.3 IR UWB Pulse Generation……....14

2.4 UWB Channels……..19

2.5 Advantages of IR UWB Technology……..……20

2.6 Applications of Ultra-wideband.……....24

2.6.1 High Data Rate- Communication Applications…….……...25

2.6.2 Low Data Rate- Positioning Applications…….……...26

2.6.3 Radar Applications……..……..26

2.7 Challenges of UWB…….……..……..26

CHAPTER 3 IR UWB IMPLEMENTATION SCHEMES……28

3.1 Rake Receiver……..……..28

3.2 Transmit Reference Scheme…….……30

3.3 Frequency Shift Reference Scheme……...31

3.4 Code Shift Reference Scheme……..……32

3.4.1 CSR Transmitter Structure……33

3.4.2 CSR Receiver Structure……....34

3.5 Differential Code Shift Reference Scheme…..…….……36

3.5.1 DCSR Transmitter Structure…….……37

3.5.2 DCSR Receiver Structure…….38

3.6 DCSR Encoding: An Example……..……40

3.7 Performance Comparisons between IR Schemes……...……..…….41

CHAPTER 4 DCSR UWB TRANSCEIVER STRUCTURE……...……..……47

4.1 DCSR Transmitter…….……47

4.2 DCSR Receiver…….……...….50

4.3 Nonlinearity of Transmitter RF Mixer…….…….……54

4.4 Circuit Level Modifications to Overcome Mixer Nonlinearity…….……..57

CHAPTER 5 THE PROPOSED TRANSMITTER TEST SEQUENCE

GENERATION AND BIT ERROR RATE TESTS…..…….....…….61

5.1 Existing Data Bit Generation in DCSR Transmitter….....61

5.2 Bit Error Rate Tester…….……63

5.3 Test Sequence Generation for Bit Error Rate Tests……...…….…….64

5.4 Bit Error Rate Tests in Practical Environments ……...……...……...70

5.4.1 BER Results in ideal LOS Environment ……...…….....…..71

5.4.2 BER Results in Multipath LOS Environment……...73

CHAPTER 6 CONCLUSION AND FUTURE WORK…….78

6.1 Conclusion……78

6.2 Future Work……..79

REFERENCES…….80

LIST OF TABLES

Table 2.1: Emission levels of popular wireless communication systems [2]……..…….8

Table 2.2: EIRP levels authorised by FCC for indoor and outdoor

UWB systems [13]…….....10

Table 2.3: Channel modelling for IEEE 802.15.4a [32]…….....20

Table 3.1: CSR shifting and detection codes [3]…….....36

Table 3.2: DCSR shifting and detection codes [4]…….....40

Table 3.3: All possible DCSR encoding patterns, when $N_f = 4$……...41

Table 3.4: Comparisons between TR, FSR, CSR and DCSR [6]……...….46

Table 5.1: Binary test sequence generation from ‘word’ format in BERT……67

Table 5.2: BER test results in ideal LOS environment……..…...72

Table 5.3: BER test results in multipath LOS environment…….....74

LIST OF FIGURES

Figure 2.1: FCC defined UWB bandwidth requirements [1]……...7

Figure 2.2 (a): Emission standards for UWB indoor communications [1]……...…....9

Figure 2.2 (b): Emission standards for UWB outdoor communications [1]…….....9

Figure 2.3: Multi Band OFDM frequency band plan…….……11

Figure 2.4: Comparison between narrowband, wideband & IR schemes [33]……..…..13

Figure 2.5: Gaussian pulses of width 'T_p' in time domain……..……16

Figure 2.6: First three derivatives of Gaussian pulse in time domain…….....17

Figure 2.7 (a): n^{th} order Gaussian pulses with 't_p' pulse widths,

in time domain [24]…….....17

Figure 2.7 (b): n^{th} order Gaussian pulses with 't_p' pulse widths,

frequency domain [24]……...18

Figure 2.8: Co-existence of UWB with narrowband and wideband [2]…….….21

Figure 2.9: Duty cycle of an impulse radio……..…….....22

Figure 2.10: A multipath indoor wireless channel condition [2]……23

Figure 2.11: UWB vs other IEEE wireless standards…….25

Figure 3.1: Structure of Rake receiver [35]……....28

Figure 3.2: All Rake receiver [13]……..29

Figure 3.3: Selective Rake receiver [13]……30

Figure 3.4: TR receiver structure [33]……31

Figure 3.5: Structure of FSR receiver [36] ……32

Figure 3.6: Structure of CSR UWB transmitter [3]……33

Figure 3.7: CSR UWB receiver structure [3]……..……...35

Figure 3.8: Structure of DCSR UWB transmitter [4]……..……...37

Figure 3.9: DCSR UWB receiver structure [4]……..……38

Figure 3.10: Theoretical vs simulation BER analysis for CSR

UWB System [5]…….…....43

Figure 3.11: Theoretical vs simulation BER analysis for DCSR

UWB System [6]…….……..43

Figure 3.12: BER performance simulations for TR, FSR, CSR and DCSR,

when *M*=2 [6]……...44

Figure 3.13: BER performance simulations for TR, FSR, CSR and DCSR,

when *M*=3 [6]……...45

Figure 4.1: DCSR transmitter structure…….47

Figure 4.2: DCSR data modulated clocks from FPGA [7] [8]……..……..48

Figure 4.3: DCSR pulse generator outputs [8]…….……..49

Figure 4.4: Main blocks of DCSR receiver [7] [8] [10] [11]…...…….....51

Figure 4.5: Signal recovery stage [8] [12]…….……..……..52

Figure 4.6: High frequency removal stage [7] [8]……..……..……..53

Figure 4.7: Detection and decoding stage [10] [11]…….…..…54

Figure 4.8: Structure of inverting Op Amp…….……...54

Figure 4.9: Pulse amplitude modulation circuit using ADS [8]…….....55

Figure 4.10: Pulse amplitude modulation stage simulation output [8]…….....55

Figure 4.11: RF mixing stage simulation output [8]……..56

Figure 4.12: Pulse ratio at the output of DCSR transmitter……..…….57

Figure 4.13: ADS simulation results for (a) output of Op Amp 1,

(b) output of Op Amp 2 and (c) pulse combiner output……58

Figure 4.14: Modified pulse amplitude modulation stage output……...59

Figure 4.15: Desired pulse ratio after RF mixer stage…….……...……59

Figure 4.16: Output of DCSR transmitter before antenna…….60

Figure 5.1: DCSR encoding simulations: Corresponding to data bit sequence……..62

Figure 5.2: DCSR encoding simulations: Corresponding to pulse generation…..……...63

Figure 5.3: ‘generator’ and ‘analyzer’ of BERT……..…….……64

Figure 5.4: DCSR data modulation when bits *b*=0……65

Figure 5.5: Generated test data sequence by BERT (2 cycles)……..68

Figure 5.6: Test data sequences at ‘generator’ and ‘analyzer’ of BERT……69

Figure 5.7: BER test setup of DCSR transceiver…….……..70

Figure 5.8: BER inside anechoic chamber when distance
between antennas is 2.5 meters……...73

Figure 5.9: BER results in multipath LOS environment when antennas distance
is: (a) 0.05 meter; (b) 1 meter; (c) 2 meters and (d) 3 meters…….76

Figure 5.10: BER result assessments: Ideal and Multipath LOS Environments……..77

ABSTRACT

Impulse radio is a wireless communication technique in which ultra-short pulses in the range of nano-seconds are used for the transmission of information. These ultrashort pulses spread over the radio frequency spectrum covering wide range of frequency bands, creating an ultra-wideband signal. Using impulse radio makes a wireless communication system low power consuming, less complex and more immune to interference compared to sinusoidal wave based systems. Additionally, ultra-wideband offers several advantages like high data rate and ability to work under low signal to noise ratio. Therefore, many modulation schemes have been developed in order to exploit the advantages offered by impulse radio ultra-wideband, after the commercialization of ultra-wideband technology by Federal Communication Commission in 2002.

To overcome the disadvantages of existing impulse radio ultra-wideband modulation schemes, new improved Code Shift Reference schemes were proposed by our research group. Differential Code Shift Reference is one among the Code Shift Reference schemes in which the data is differentially encoded using impulse radio pulses. A prototype transceiver was developed using Differential Code Shifted Reference scheme. The transmitter uses 4 ns durational impulses to carry information. The pulses have the pulse repetition rate of 20 MHz and the bandwidth of 500 MHz, centered at 4.44 GHz. The original information is extracted from the encoded pulses according to Differential Code Shift Reference decoding algorithms in the receiver.

This thesis presents the bit error rate testing of the Differential Code Shift Reference ultra-wideband transceiver, which has not been well addressed before. Circuit level modifications were done in the transmitter to address the issue of nonlinearity. To conduct bit error rate tests, a new way of test sequence generation is proposed and the Differential Code Shift Reference encoding module in transmitter was modified to use the generated test sequences for modulation. Tests were conducted using two different wireless environments. The results from the bit error rate tests demonstrated that the system functions as it should be, meeting the theoretical design expectations.

LIST OF ABBREVIATIONS AND SYMBOLS USED

AGC	Automatic Gain Control
ADC	Analog to Digital Converter
ADS	Advanced Design System
AM	Amplitude Modulation
AWGN	Additive White Gaussian Noise
BER	Bit Error Rate
BERT	Bit Error Rate Tester
BPF	Band Pass Filter
BPS	Bits per Second
BW	Bandwidth
CMOS	Carbon Metal Oxide Semiconductor
CSR	Code Shifted Reference
dB	Decibels
dBm	Decibels-Milliwatts
DCSR	Differential Code Shifted Reference
DS UWB	Direct Sequence Spread Spectrum Ultra-wideband
EIRP	Equivalent Isotropic Radiated Power
FCC	Federal Communications Commission
FPGA	Field Programmable Gate Array
FSR	Frequency Shifted Reference
GPS	Global Positioning System
GHz	Gigahertz

HDR	High Data Rate
Hz	Hertz
IC	Integrated Circuit
IR	Impulse Radio
ISI	Inter Symbol Interference
KBPS	Kilo Bits per Second
KHz	Kilo Hertz
LAN	Local Area Network
LDR	Low Data Rate
LFSR	Linear Feedback Shift Register
LNA	Low Noise Amplifier
LOS	Line of Sight
LPF	Low Pass Filter
LSB	Least Significant Bit
MAC	Media Access Control
MAN	Metropolitan Area Network
MBPS	Mega Bits per Second
MHz	Mega Hertz
MOSFET	Metal Oxide Semiconductor Field-Effect Transistor
MPC	Multipath Component
MSB	Most Significant Bit
NLOS	Non Line of Sight
OFDM	Orthogonal Frequency Division Multiplexing
OOK	On-Off Key

PAM	Pulse Amplitude Modulation
PAPR	Peak to Average Power Ratio.
PCB	Printed Circuit Board
PLL	Phase Lock Loop
PRBS	Pseudo Random Bit Sequence
PRR	Pulse Repetition Rate
PRN	Pseudo Random Number
PSD	Power Spectral Density
RF	Radio Frequency
SNR	Signal to Noise Ratio
TH UWB	Time Hopping Ultra-wideband
TOA	Time of Arrival
TR	Transmitted Reference
UWB	Ultra-wideband
VCO	Voltage Controlled Oscillator
VCXO	Voltage Controlled Crystal Oscillator
VGA	Variable Gain Amplifier
VHDL	Very-High-Speed-Integrated Hardware Description Language
WLAN	Wireless Local Area Network
WPAN	Wireless Personal Area Network

ACKNOWLEDGMENTS

I would like to express my heartfelt appreciation to my supervisor Dr. Zhizhang Chen for accepting me as his graduate student and providing me the opportunity to work in the interesting research topic of UWB communications. His patient guidance, enthusiastic support and useful critiques during the progress of this thesis are deeply appreciated. Also, I'm greatly thankful for my co-supervisor Dr. Hong Nie for sharing his immense knowledge of UWB with me by providing the vital suggestions and corrections during the progress of this thesis. Those corrections played vital role in the successful completion of the work.

I'm particularly grateful to my committee members Dr. Kamal El-Sankary and Dr. William J. Phillips, for spending their valuable time during my defence, their advice and the corrections. I would like to extend my gratitude to all faculty members in Electrical & Computer Engineering department for their help in offering me various resources and fine tuning my skill sets.

Completion of this thesis could not have been accomplished without the support of my colleagues in RF/Microwave wireless research lab. Special thanks to Mingwei Liu and Colin O'Flynn for their co-operation and valuable feedbacks during the thesis work. Help of staff members and lab technicians in the Electrical & Computer Engineering department is greatly appreciated.

I also like to thank Dr. Jose Gonzalez-Cueto, assistant professor in department of Electrical & Computer Engineering for offering me the teaching assistant and marker positions during my studies. They were very valuable work experiences and I enjoyed a lot.

Last but the most important, I am very grateful for my parents for all the love, support and motivation during my graduate degree in Canada. Big thanks to all my friends and colleagues of RF & Microwave research group who made my stay in Halifax very joyful and memorable years of my life.

CHAPTER 1 INTRODUCTION

This chapter presents background, history, timeline of growth, advantages and research motivations for impulse radio wireless communication technology. This chapter ends with the outline of the thesis.

1.1 Impulse Radio Background

Since its birth during the latter half of 19th century, wireless communication technology has grown rapidly over the years to meet ever growing consumer demand. This rapid growth has led to the evolution of various radio technologies for both military and commercial applications. All these radio technologies have become more and more 'sophisticated'- faster, secure and well refined in due course. However, most of these technologies use narrowband continuous waves for wireless transmission, a conventional method used for radio transmissions during past century.

To avoid interference with each other, each existing narrowband system is allocated in a specific part of the radio frequency (RF) spectrum. As a limited constant resource, RF spectrum becomes more and more crowded with the introduction of each new radio application. Decreasing the bandwidth to overcome this spectral congestion not only limits the capacity of the system (Shannon's theorem) but also increases the interference with neighbouring systems.

To address the problem of ever-growing spectral congestion, many new techniques like impulse radio and cognitive radio have been introduced in recent years. These techniques mainly focus on improving the spectrum utilization efficiency, such that a new system can co-exist with an existing system by sharing the same frequency bands, without quality and/or performance trade-offs. In particular, impulse radio (IR) technique has been emerged as an alternative to traditional narrowband wireless technology in recent years due to its simplicity, signal properties and the availability of massive spectral resources for commercial applications.

Although impulse radio attracted much of its attention in recent years, the technology itself is not something new. All the primitive wireless systems were in fact impulse based. Carbon electrode was used as an electromagnetic pulse generator to generate arc discharges during Herich Hertz's early day communication experiments in 1893. Today those arc discharges are categorized as coloured noise. By using the pulses generated by a spark gap transmitter, the first trans-Atlantic wireless communication was successfully demonstrated by Gugliemo Marconi in 1901. As wireless technology started to evolve, sinusoidal wave based narrowband communication systems became predominant due to spectral and technical difficulties involving short durational pulses. There was hardly any pulse based communication system apart from telegraphy for many decades. However, advancements in solid state electronics during 1960s began to eliminate the difficulties associated with generation of ultra-short pulses. At the same time, development of sampling oscilloscope initialized the work of characterizing transient behaviour of impulse radio. Experimental results demonstrated that ultra-short pulses can provide more accuracy, better interception avoidance and have better penetrating properties. As a result, impulse radio was extensively used in military radars. Other applications such as collision avoidance, positioning and altimetry were also developed during late twentieth century. Primarily these developments were done either by the military or by classified defense programs funded by the government [2].

1.2 Research Motivation

Historically used in military applications, impulse radio had very little significance in commercial applications before 2002 due to RF spectrum licence restrictions. This is because, ultra-short pulses occupy wide bandwidth in the spectrum-sometimes up to several GHz, depending on the pulse duration, making an ultra-wideband system. For commercial applications, obtaining a part in RF spectrum which contains GHz range bandwidth was difficult because of the tight regulations by spectral allocation authorities around the world. This lead to the domination of narrowband wireless technology. However, The First Report and Order [1], released by Federal Communication

Commission (FCC) in 2002 unlicensed two parts of RF spectrum for ultra-wideband (UWB) commercial applications. This report also defined the definition of UWB communications and set the ground rules for its commercial use. Since then UWB radio has attracted significant attention from both industry and academia to exploit the advantages offered by wide bandwidth and to effectively address the challenges encountered by sinusoidal wave based systems.

Although UWB signaling can be done using many wireless modulation methods, single band impulse radio has been emerged as one of the prominent method during recent years. The ultra-short pulses used in IR UWB are generally of nanosecond/sub-nanosecond durational and they spread widely across the RF spectrum, covering several frequency bands. Using these ultra-short pulses in impulse radio offers key benefits like massive bandwidth, low signal to noise ratio requirement, simple design requirements, low power consumption, low equipment cost, multipath immunity, better accuracy, superior penetrating properties, low probability of detection and ranging & communication at the same time [2].

Regardless of countless advantages, using ultra-short pulses pose a unique problem during the design of IR UWB transceiver. A conventional IR UWB receiver design becomes complex in multipath environments due to the requirements of channel estimation and tracking. Literatures do provide alternative implementations such as Transmit Reference (TR) and Frequency Shift Reference (FSR), which involve in the separation of reference and data pulse sequences by time and frequency shifts respectively. However, when it comes transceiver implementation, both TR and FSR schemes are difficult to realise, suffering from complex architectural requirements and performance trade-offs.

To overcome the above mentioned difficulties, new code shifting schemes with better performance, like Code Shift Reference (CSR) [3] and its improved version, Differential Code Shift Reference (DCSR) [4] have been proposed recently. In CSR and DCSR schemes, data sequences are separated from reference sequences using specific shift codes, such as Walsh codes. In the receiver, information bits are extracted from pulse sequence

using detection codes. Code shift schemes eliminate the requirements of channel estimation, delay element and analog carrier, leading to system simplicity. Simulation results in [5] and [6] have shown that code shift schemes achieve superior performance and provide better bit error rate results compared to TR and FSR. These advantages make code shift schemes more appealing topics for further research and implementation.

Literatures from [7] to [12] discuss the detailed developmental process of a prototype DCSR IR UWB transceiver. In all the reports so far, not much have been done on the bit error rate tests and the performance analysis of the implemented transceiver. This thesis emphasizes on the subsequent necessary works, which were done to analyze the bit error rate performance of the transceiver. They are, (i) achieving the desired DCSR pulse ratio at the transmitter output, which reduces due to the nonlinear characteristics of wideband RF circuit elements used in transmitter, (ii) replacing the existing digital data bit generation scheme with externally geneated test sequences and modifying the DCSR encoding module of transmitter to use the externally geneated test sequences for DCSR encoding (iii) proposing a new way of test sequence generation using bit error rate tester and (iv) conducting the BER tests in two different wireless communication channels. The obtained results show that the DCSR transceiver can work satisfactorily in realistic wireless applications.

1.3 Outline of the Thesis

Chapter 1 discussed the problems which led to the growth of alternative wireless communication methods, history and timeline of growth of impulse based wireless communications. Advantages of using impulse radio ultra-wideband and the drawbacks of popular existing impulse radio modulation schemes, which motivated the development of new code shifting reference schemes were also discussed briefly.

Chapter 2 presents definitions and signaling regulation guidelines set by FCC for commercial UWB systems. Then two prominent methods of UWB signaling, Impulse

Radio (IR) and Multi Band Orthogonal Frequency Division Multiplexing (MB-OFDM) will be explained. Since impulse radio ultra-wideband is the technology used in this thesis, pulse generation, properties, advantages and potential applications of IR UWB in near future are presented.

Chapter 3 reviews the literatures of some popular IR UWB implementation schemes. Rake receiver, the most common IR UWB receiver scheme is investigated first. Following Rake receiver, other non-coherent schemes like Transmit Reference, Frequency Shift Reference are studied. New novel code shift schemes such as Code Shift Reference and Differential Code Shift Reference are reviewed in later sections of the chapter. The chapter ends with comparing the performances among TR, FSR, CSR & DCSR schemes.

Chapter 4 describes the structure and functions of existing DCSR IR UWB transceiver blocks in detail. Chapter also provides the work done on optimizing the DCSR transmitter performance to conduct bit error rate tests. Necessary changes made at the pulse amplitude modulation (PAM) stage of the transmitter to achieve desired pulse ratio are presented in this chapter.

Chapter 5 covers the bit error rate test set up, procedures and bit error rate results of DCSR IR UWB transceiver. A new way of test sequence generation to conduct bit error rate tests is proposed in this chapter. Bit error rate measurements are conducted in both ideal wireless testing environment in the absence of multipath and in the standard laboratory environment. Results are tabulated and analyzed.

Chapter 6 is the final chapter which concludes this thesis. Necessary works which need to be addressed in the near future are also mentioned.

References for this thesis work are listed after final chapter.

CHAPTER 2 UWB DEFINITIONS AND SIGNALING METHODS

A comprehensive overview of UWB signaling regulations set by FCC for its commercial use is presented in this chapter. Popular UWB signaling methods, with emphasis on IR-UWB are also discussed. Later sections in chapter mention IR UWB signal generation, its advantages, applications and potential challenges as well.

2.1 FCC Regulations

As mentioned earlier in the first chapter, commercial applications were heavily restricted from using large GHz range bandwidth due to the spectral allocation difficulties until 2002. However, The First Report and Order, published by FCC in 2002 [1], unlicensed the two RF frequency bands, DC-960 MHz and 3.1 GHz-10.6 GHz for the use of commercial UWB applications. FCC also set specific bandwidth and emission level requirements for UWB communications. Following FCC, most regional spectrum regulatory authorities around the world also unlicensed parts of radio spectrum for commercial UWB systems, though frequency bands and emission levels slightly vary across the countries. UWB spectral regulations are much more relaxed in US and Canada, where as in Europe and Asia, they are strictly followed.

According to FCC report, a wireless technology is termed as ultra-wideband, only if its signals have,

a. An absolute bandwidth (BW) of at least 500 MHz. Absolute bandwidth is the difference between the highest (f_H) and the lowest (f_L) frequency components of the signal, measured at -10dB below from the strongest frequency component in the signal spectrum. Absolute bandwidth is given by,

$$(f_H \sim f_L) = BW \geq 500 \text{ MHz} \tag{2.1}$$

Or

b. A fractional bandwidth (B_f) of at least 20% of the center frequency (f_c) of the signal spectrum. Fractional bandwidth is determined from bandwidth using the equation,

$$B_f = \frac{BW}{f_c} \geq 20\% \qquad \text{where, } f_c = \frac{f_H + f_L}{2} \tag{2.2}$$

Figure 2.1 explains the minimum absolute and relative bandwidth requirements for commercial UWB communications, as defined by FCC.

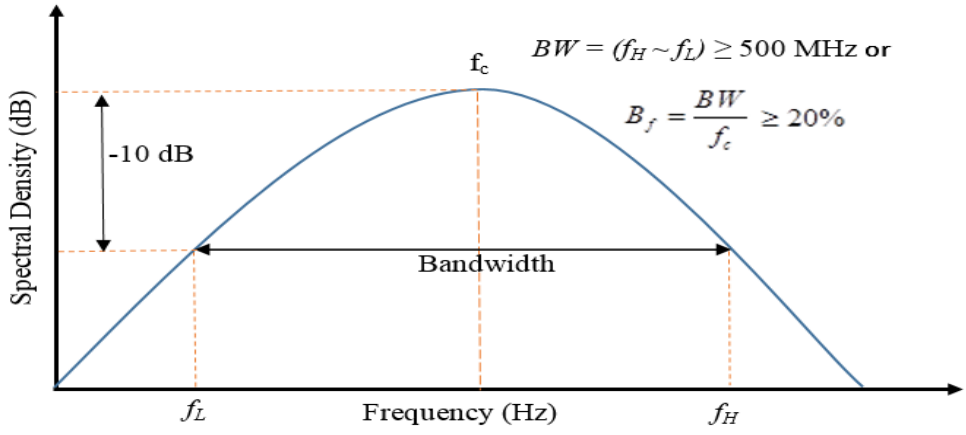

Figure 2.1: FCC defined UWB bandwidth requirements [1]

As UWB signals generally occupy several frequency bands, sometimes in the range of GHz, sharing the RF spectrum along with other communication systems becomes inevitable, which undoubtedly leads to severe interference. To make this co-existence possible with minimal or no interference, FCC has set very low power spectral density level for UWB, which falls under the noise floors of most existing narrowband systems [1]. Power spectral density is the ratio between the total power transmitted by the transmitter (P in Watts) and its signal bandwidth (BW in Hertz), which is given by,

$$PSD = P/BW \tag{2.3}$$

FCC allowed a maximum equivalent isotropic radiated power (EIRP) of -41.3 dBm/MHz (or 74.13 nW/MHz) for commercial UWB applications [1]. EIRP is the total power

radiated by an antenna, assuming the antenna is an isotropic radiator. EIRP is determined from the equation,

$$EIRP = P_T - L_S + G_A \tag{2.4}$$

where, P_T is transmitter power, L_S is the loss in the system and G_A is the maximum gain of the antenna. Table 2.1 compares the emission level of UWB with other popular continuous wave wireless systems [2].

Communication System	**Bandwidth**	**Total Power Transmitted**	**Power Spectral Density**
AM Radio	75 KHz	50 kW	666 X10^3 W/MHz
Television	6 MHz	100 kW	16 X 10^3 W/MHz
Cellular Systems	8.33 kHz	500 mW	60 W/MHz
Broadband Wi-Fi	20 MHz	1 W	0.05 W/MHz
UWB	7.5 GHz	0.5 mW	6.67 X10^{-8} W/MHz

Table 2.1: Emission levels of popular wireless communication systems [2]

As it can be seen from the above table, even with the complete utilization of 3.1-10.6 GHz frequency bands, the maximum total power that an UWB transmitter can emit is only about 0.5 mW. Plots in Figure 2.2 (a) and (b) show the FCC authorised EIRP standards for indoor and outdoor UWB commercial applications respectively. Similar emission level standards are established worldwide by other spectrum regulatory authorities and are often updated according to spectrum availability and other regional requirements.

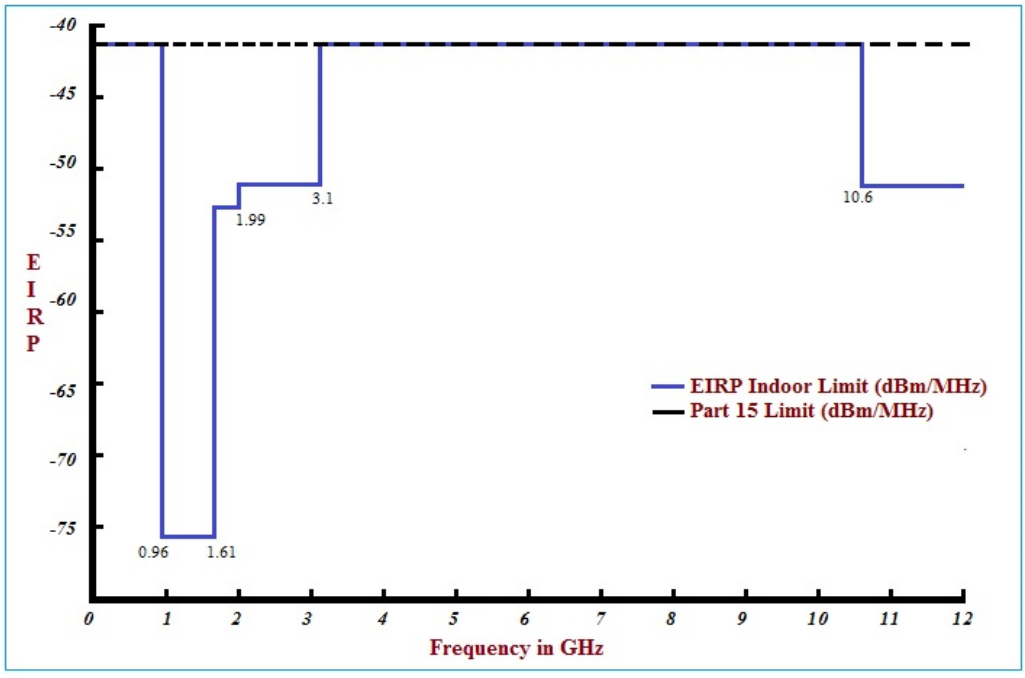

Figure 2.2 (a): Emission standards for UWB indoor communications [1]

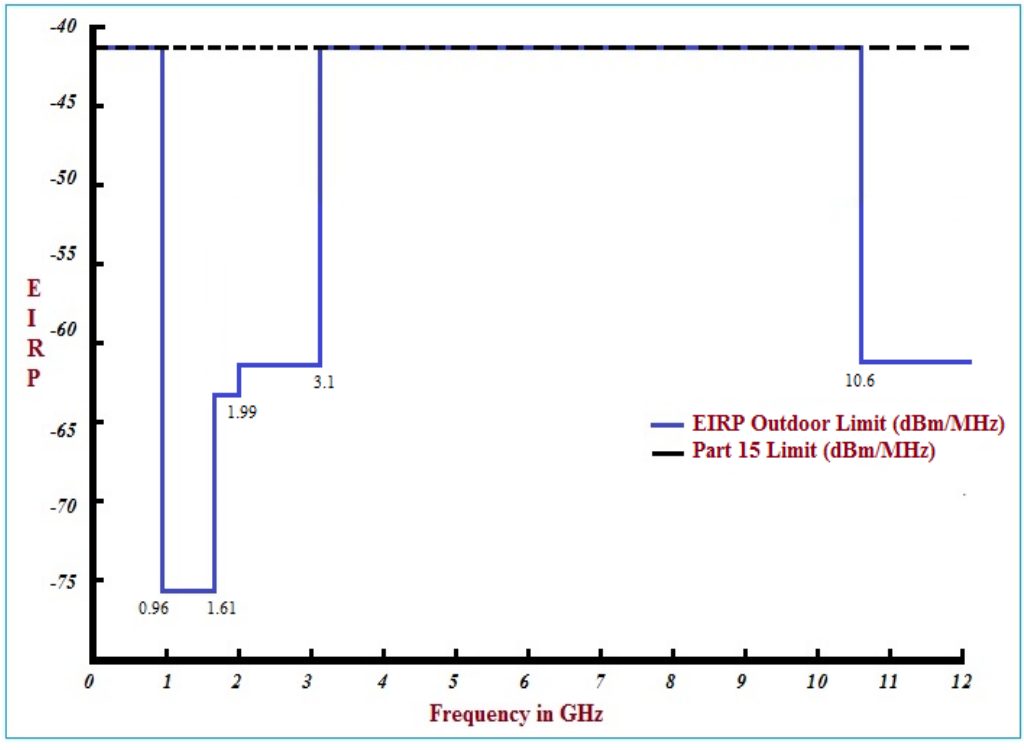

Figure 2.2 (b): Emission standards for UWB outdoor communications [1]

The maximum EIRP (dBm/MHz) levels at different frequency bands across the RF spectrum, authorized by FCC for commercial UWB are summarized in Table 2.2.

Frequency in GHz	**Indoor EIRP**	**Outdoor EIRP**
< 0.96	**- 41.3**	**-41.3**
0.96 – 1.61	-75.3	-75.3
1.61 – 1.99	-53.3	-63.3
1.99 – 3.1	-51.3	-61.3
3.1 – 10.6	**-41.3**	**-41.3**
> 10.6	-51.3	-61.3

Table 2.2: EIRP levels authorised by FCC for indoor and outdoor UWB systems [13]

Unlicensed frequency bands from DC-960 MHz can be used for low data rate (LDR) UWB applications. The EIRP is set to extremely low level (-75.3 dBm/MHz) for the part of the RF spectrum from 0.96-1.61 GHz. This is to safeguard the UWB system's signals against the potential interference from the signals of Global Positioning System (GPS), since power spectral density of GPS signals come under similar range. Thus, the main frequency bands which can be used by the UWB commercial applications of high data rate (HDR), which is the key benefit of UWB, lies between 3.1-10.6 GHz [15]. However, to avoid the possibility of any interference from signals of wireless local area network (WLAN 802.11a) operating at 5 GHz range, it is ideal to use either a lower frequency bands of 3.1-5.0 GHz or upper frequency bands of 6.0-10.6 GHz during the development of UWB communication system.

2.2 UWB Signaling Schemes

Since commercial UWB is deregulated and can be used freely, various signaling schemes have been developed over the years. However, efforts to establish standards have been made by organizations like IEEE LAN/MAN Standards Committee to provide the compliance between devices using various UWB schemes. One of such standardization is the development of high data rate Multi Band Orthogonal Frequency Division Multiplexing (MB-OFDM) by Task Groups 3 and 4 of IEEE 802.15 committee. The task group 802.15.3a in [14] attempted to standardize high data rate UWB using either impulse radio Direct Sequence Ultra-wideband (DS UWB) or Multi Band Orthogonal Frequency Division Multiplexing (MB-OFDM) signaling modes. Another task group, 802.15.4a in [16] proposed a low data rate physical layer standard using UWB for wireless personal area network (WPAN) with precision ranging capability. While these regulations are not yet universally accepted, least they attempt to standardize UWB system development.

2.2.1 MB Orthogonal Frequency Division Multiplexing

Multi Band OFDM is a carrier based UWB communication scheme which was initially supported by MB OFDM Alliance (now MBOA, a part of WiMedia Alliance). In this scheme, the entire 3.1-10.6 GHz UWB spectrum has been split into 14 uniform sub-bands, clustered using five groups. Each sub-band has a bandwidth of 528 MHz, as shown in the Figure. 2.3 [17].

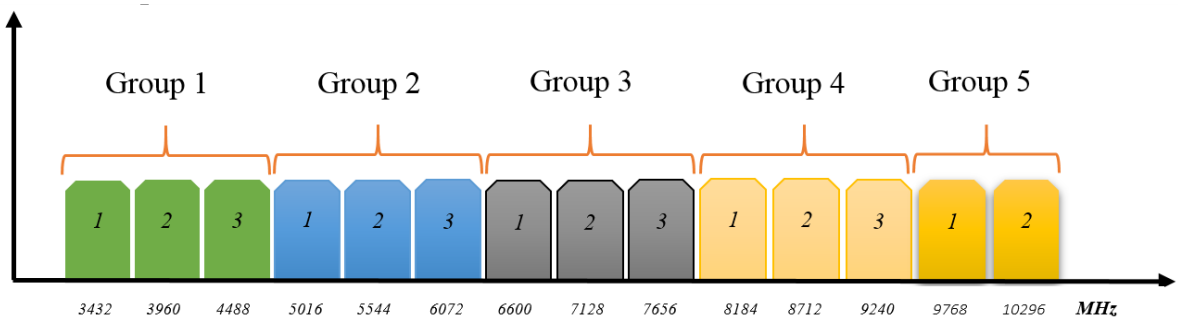

Figure 2.3: Multi Band OFDM frequency band plan

The information bit stream is split into several sub-streams and is inserted in OFDM sub-bands as low data rate parallel streams. Each parallel stream is modulated using separate parallel (but orthogonal) sub-carrier. Since subcarriers are spaced in such a way that they are orthogonal to each other, overlapping is possible, resulting in highly efficient spectrum modulation [18]. The multiband design of MB-OFDM also offers flexibility while designing the UWB systems, from the varying spectrum regulations of different regions around the world [19]. To co-exist with a narrow band system without interference, one of the bands or a group of MB-OFDM can be removed from the system with minimum performance degradation. For instance, to mitigate the signal distortions from WLAN (802.11a) at 5 GHz, Group #2 or one of its sub bands can be turned off. Symbol period of each sub-band in MB OFDM is longer compared to impulse radio, minimizing the inter-symbol interference (ISI) and increasing the multipath immunity [19]. However, complexity of the transceiver structure increases in MB-OFDM with the increase in data rate. This leads to the requirements of powerful processing engines and more power, although synchronization is easier.

2.2.2 Impulse Radio Ultra-wideband

As it has been discussed briefly before, IR UWB schemes use ultra-short pulses of nano/sub-nanoseconds duration for signaling. Though these pulses do not carry any data within themselves, data is encoded in the pulse sequence using one of the available impulse radio modulation schemes like position, polarity etc. Figure 2.4 compares IR UWB with conventional wireless schemes in time and frequency domains respectively.

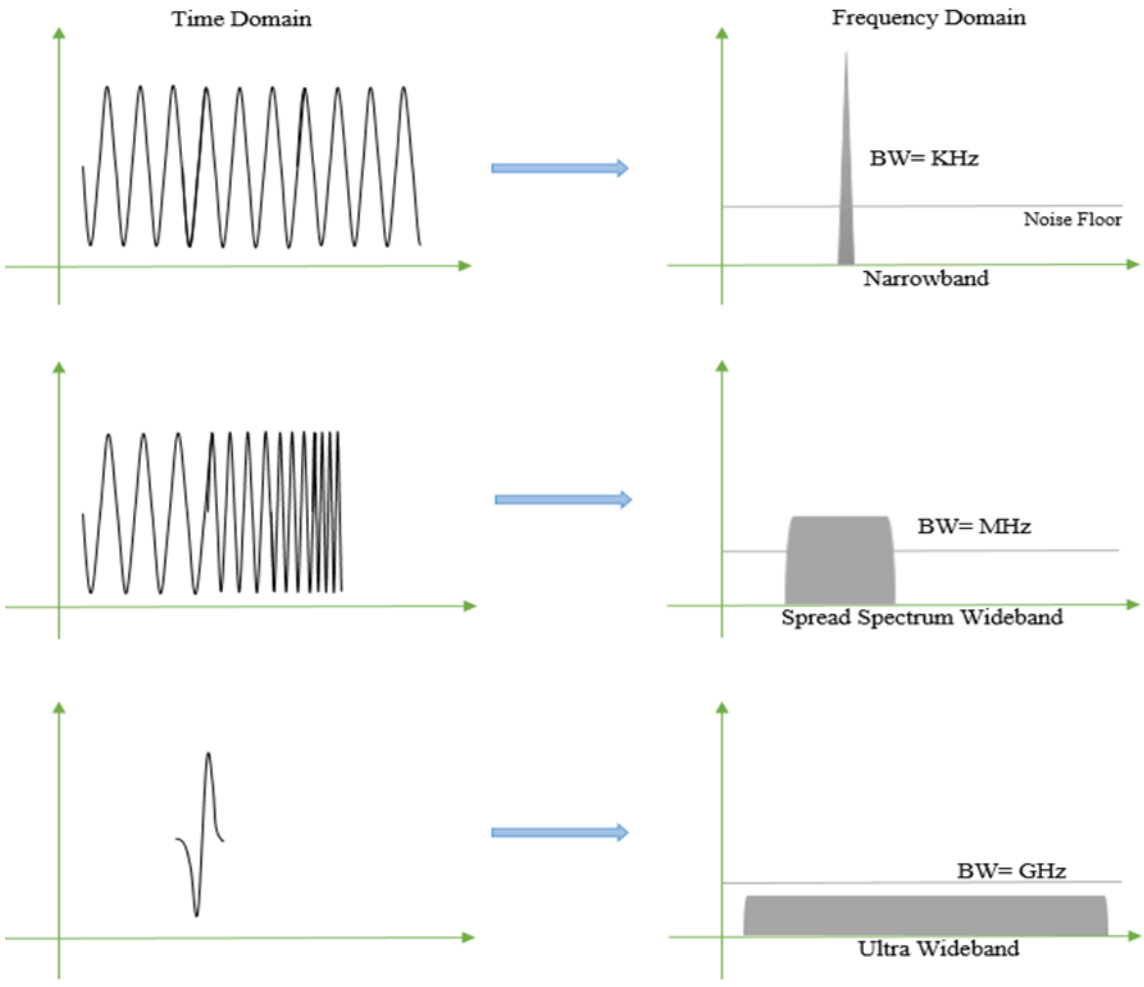

Figure 2.4: Comparison between narrowband, wideband & IR schemes [33]

Direct Sequence Ultra-wideband (DS UWB) and Time Hopping Ultra-wideband (TH UWB) are two prominent subcategories of IR UWB [20]. In DS UWB, data encoded IR pulses are transmitted continuously (but each user is allocated with different pseudorandom sequences). In TH UWB, data encoded IR pulses are transmitted only in specific allocated time slots for each user.

IR UWB can be implemented either as carrier less or carrier based [18]. In carrier less IR UWB, impulse signal is generated in such a way that the baseband pulses are already in RF range, eliminating the carrier requirement for wireless channel transmission. Without the carrier signal, the requirements of oscillator, mixer and steps involved with RF up/down conversions are eliminated. This keeps the transceiver structure simple.

In carrier based IR UWB, the signal is generated by mixing a higher frequency carrier, uplifting the energy DC range to a targeted UWB band in the RF spectrum [18]. The carrier based IR UWB can be implemented either by the up-conversion of baseband pulses to a desired band in the UWB RF spectrum or by direct on-off switching operation on the oscillator itself while generating pulses [18]. The carrier based IR UWB has few advantages, a) better spectral efficiency is achieved, which increases system capacity and b) accurate timing resolution is possible with less signal processing steps at the receiver, especially in quadrature receivers [21].

However, using the carrier increases the power consumption and results in complex IR UWB transceiver architecture. Also, generating a carrier which can cover wide bandwidth becomes problematic at high frequencies [18].

2.3 IR UWB Pulse Generation

For IR UWB, it is necessary consider FCC bandwidth requirement and maximum EIRP level while generating the pulses. As approximate relationship between pulse duration (τ) and bandwidth (BW) of the impulse radio is given by,

$$BW \approx \frac{1}{\tau} \tag{2.5}$$

Thus, in order to achieve the FCC required minimum bandwidth of 500 MHz and above, the pulse width should be extremely small, in the range between sub-nanoseconds to few nanoseconds. Another primary factor, maximum permissible EIRP for commercial UWB is -41.3 dBm/MHz. EIRP is dependent on the amplitude of the IR pulses and pulse repetition rate (PRR). Power spectral density of an impulse based technology is given by [22],

$$v_f = v_t\left[\frac{\tau}{T}\right] \tag{2.6}$$

where, v_f is the power spectral amplitude of the signal spectrum, v_t refers to RMS amplitude of the pulses, Γ is the width of the pulses and T being the pulse repetition rate.

Due to ultrashort pulses, IR UWB signal's duty cycle is very low, which makes it easier to increase the PRR, which in turn increases the PSD. To keep the PSD within FCC limits, amplitude of the pulses can be lowered. In simple words, PRR and energy in each IR pulse can be tuned depending on the application requirements. This provides two application scenarios [19]:

a). **Low data rate applications**: Pulses with high energy and low PRR, which will increase the system's communication range with data rate trade-off.

b). **High data rate applications:** Low energy pulses with high PRR, which will increase the system's data rate with the communication range trade-off.

FCC hasn't defined any specific pulse shape for IR UWB communications. So any pulse shape which follows FCC defined UWB emission limit and bandwidth requirement can be used. Apart from meeting the FCC requirements, it is also desirable to consider energy efficiency and performance of the system while generating the impulse radio pulses, as both the factors are closely related to pulse shape. Smoother and stable "rise" and "fall" edges of the pulse results in reduced formation of side bands (also known as side lobes). These side lobes do not carry any useful information and typically fall outside the allocated frequency range, making them undesirable part of UWB spectrum in RF band. Using appropriate pulse shape eliminates the energy wasted in the formation of side lobes and by the techniques used to supress them. Therefore, pulses like Gaussian pulse and its derivatives, Hermite pulses, Rayleigh function curve, Manchester monocycle etc. are normally used in IR UWB [24].

Among them, Gaussian pulse and its derivatives being the easiest ones to generate and ideal for signaling, are widely used in IR UWB literatures [2] [13] [23] [25] [26] [27]. Gaussian pulse and the derivatives are the category of waveforms which can be mathematically modelled using the Gauss function given in equation 2.7 [2].

$$G(x) = \frac{1}{\sqrt{2\pi\ \sigma^2}}\ e^{-\left(\frac{x^2}{2\sigma^2}\right)} \tag{2.7}$$

where, σ being standard deviation. Figure 2.5 shows the Gaussian pulses in time domain (T_p being the pulse duration). Pulses of the Figure 2.5 are mathematically represented in the equation 2.8 [2].

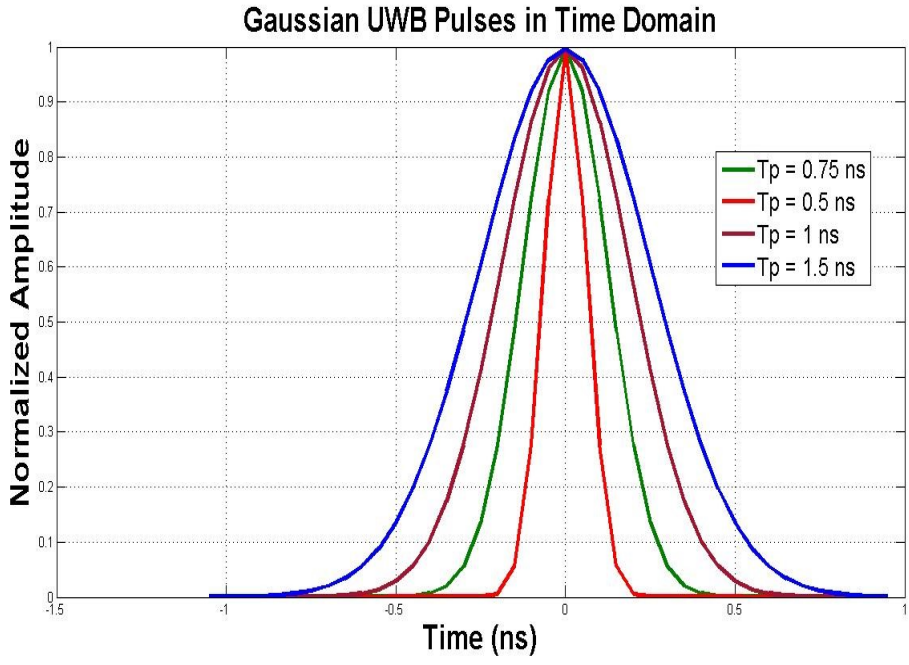

Figure 2.5: Gaussian pulses of width 'T_p' in time domain

$$y_{g1}(t) = K_1\left\{e^{\left(-\frac{t}{\tau}\right)^2}\right\} \tag{2.8}$$

in which, K_1 is a constant, τ is the time-scaling factor and time t is the pulse duration [2]. Gaussian monocycle, doublet and successive derivatives are derived from the Gaussian pulse function. Monocycle, being the first derivative of the Gaussian pulse, is expressed as [2],

$$y_{g2}(t) = K_2\frac{-2t}{\tau^2}\ \left\{e^{\left(-\frac{t}{\tau}\right)^2}\right\} \tag{2.9}$$

where, K_2 is a constant. Shapes of first three derivatives of Gaussian pulse, are provided in the Figure 2.6.

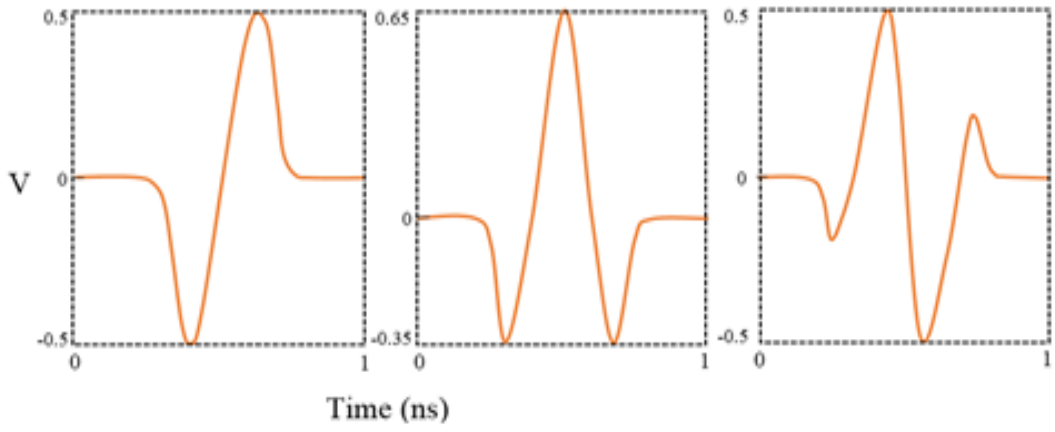

Figure 2.6: First three derivatives of Gaussian pulse in time domain

Time and frequency domain characteristics of Gaussian function pulses change significantly with reference to the order of the pulses. Literature [24] provides the detailed time and frequency domain characteristics of Gaussian pulse derivatives. It also investigates pulse propagation properties, capacity of the system using a pulse type in each scenario and the interference that a Gaussian derivative can cause to an existing system.

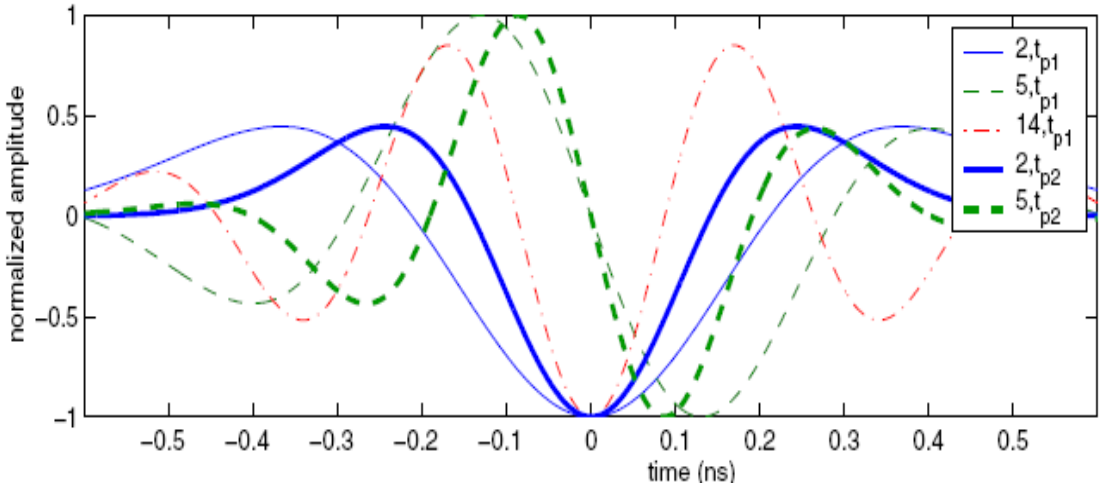

Figure 2.7 (a): n^{th} order Gaussian pulses with 't_p' pulse widths, in time domain [24]

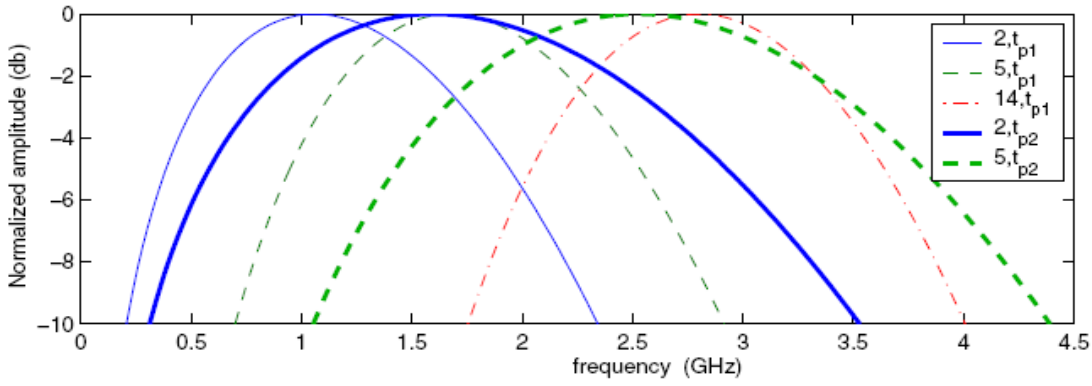

Figure 2.7 (b): n^{th} order Gaussian pulses with 't_p' pulse widths, frequency domain [24]

Figure 2.7 (a) and (b), taken from [24] provides the RF spectrum positions of Gaussian derivatives in accordance with the order of the derivatives and pulse widths (Please note '2', '5' and '14' refers to the order of Gaussian derivatives; and 't_{p1}', 't_{p2}' refers to width of the pulses).

a. Comparing 2nd, 5th and 14th order Gaussian pulses, it can be inferred that-as the order increases, pulse spectrum shifts towards higher frequency bands in the RF spectrum, with no significant change in the bandwidth.
b. For the same order Gaussian pulses, decreasing the pulse duration ($t_{p1} > t_{p2}$) increases the bandwidth.
c. Pulse spectrum shifts slightly towards higher frequency bands in the RF spectrum with the decrease in pulse duration, regardless of the order of the pulses [24].

If the UWB system is carrier less, using the higher order Gaussian derivatives should be ideal, as higher derivatives move the baseband signal from DC range to RF range [25]. However, due to the complexities involved in the generation of Gaussian pulses with higher order, most literatures prefer first two derivatives (monocycle and doublet) of Gaussian pulse for IR UWB pulse generation [26] [27] [28].

Though Gaussian monocycle and doublet do not contain any DC components and are easy to generate, their frequency bands fall below 3.1 GHz in the RF spectrum, which is outside the RF spectrum allocated by FCC for commercial UWB. This challenge can be overcome

by reducing the pulse duration, which moves the pulse spectrum to higher frequency bands above 3.1 GHz and filtering out the existing lower frequency components. Other alternative methods like using a carrier modulation and generating Gaussian pulse derivatives as a 'gated function' are also discussed in [29] and [30].

2.4 UWB Channels

Like any other signals in the wireless medium, IR UWB signals undergo attenuation and distortions in the communication channel. IR signals are also prone to fading and multipath interference, which makes the received signal at receiver considerably different from the radiated signal from transmitter. However, the channel behavior for an IR UWB signal significantly differs from that of a conventional signal. The distorted UWB signal at the receiver can be modeled as [18],

$$r(t) = \sum_{l=0}^{L-1} \alpha_l \, s\,(t-\tau_l) + n(t) \tag{2.10}$$

where, $r(t)$ is the received signal, L-the total resolvable multipath components, α_l-attenuation specific to the l^{th} path, r-l^{th} path propagation delay and $n(t)$-double sided Gaussian noise with spectral density of ($N_0/2$).

Literature [31] discusses IR UWB channel modelling extensively. One of such channel model for IEEE 802.15.4a, the subgroup mentioned in [16], which uses Saleh-Valenzuela model (SV model), is given in the Table 2.3 [32]. SV model is one of the widely used wideband propagation model which defines the resolvable multipath components' delays and amplitudes using random probability distributions [31].

Channel Model	Type	Category	Range (m)
1	Residential	Line of sight	7-20
2	Residential	Non line of sight	7-20
3	Indoor office	Line of Sight	3-28
4	Indoor office	Non line of sight	3-28
5	Out door	Line of sight	5-17
6	Out door	Non line of sight	5-17
7	Industrial	Line of sight	2-8
8	Industrial	Non line of sight	2-8
9	Open out door	Non line of sight	-

Table 2.3: Channel modelling for IEEE 802.15.4a [32]

2.5 Advantages of IR UWB Technology

Due to its large bandwidth and the nature of ultrashort pulses, using IR UWB offers variety of advantages compared to conventional narrowband technology.

Wide bandwidth and high channel capacity: The primary advantage of UWB is the availability of massive spectrum due to its relatively wide bandwidth. Using wideband results in increased channel capacity, thus, in increased data rates. According to Shannon's theorem,

$$C = BW \log_2 (1 + SNR) \tag{2.11}$$

Where, *C*-maximum channel capacity, *BW*-bandwidth and *SNR* is the signal-to-noise ratio of the system.

Therefore, a system's channel capacity can be improved linearly by increasing the bandwidth of the system or logarithmically by increasing the SNR. Depending on the operating channel's conditions, either channel capacity is increased or signal to noise ratio can be lowered. This ability to work under low signal to noise ratio provides UWB system the potential to function even under extremely noisy and unreliable channel conditions.

Co-existence: Due to very low operating EIRP of -41.3 dBm/MHz, UWB systems work below the noise floor of narrowband and spread spectrum systems. So the low power signals from UWB system are treated as noise by high power sinusoidal based wireless systems. This makes co-existence possible with minimal interference [13]. Co-existence of UWB is illustrated in the Figure 2.8.

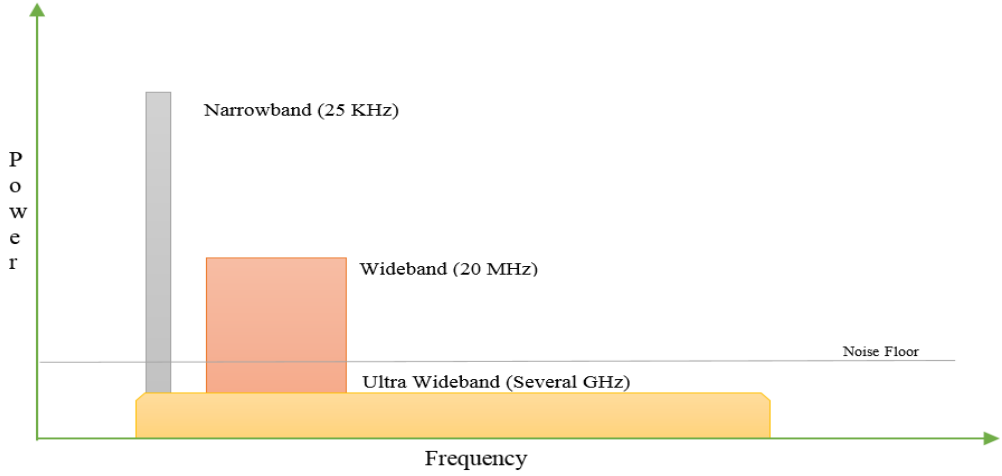

Figure 2.8: Co-existence of UWB with narrowband and wideband [2]

Flexibility: Using IR UWB offers flexibility between data rate and communication range. The duty cycle of the UWB signal is very low because of the use of ultrashort pulses for signaling. Duty cycle is given by the equation,

$$Duty\ Cycle\ =\ \frac{T_{on}}{(T_{on}+T_{off})}\times\ 100 \tag{2.12}$$

where, T_{on} is the pulse duration and T_{off} is the duration between falling edge and rising edge of two consecutive pulses, as shown in the Figure 2.9.

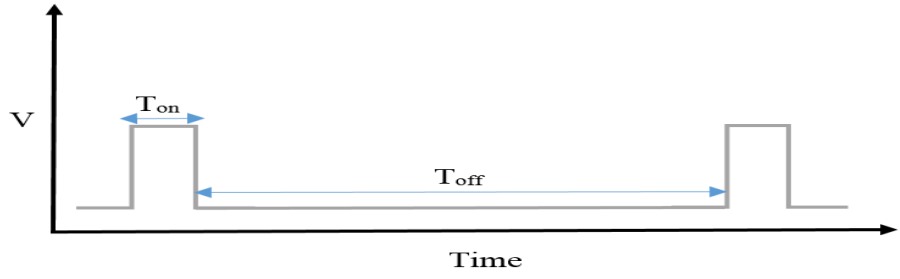

Figure 2.9: Duty cycle of an impulse radio

Because of the low duty cycle, increase in pulse repetition rate (PRR) can be achieved easily by increasing the pulse generator clock. Increase in PRR results in proportional data rate increase, along with increase in PSD of the radiated signal. To keep the signal level below the maximum permitted EIRP, power spectral density can be reduced by decreasing the energy in each pulses.

Thus, depending on the requirement, amplitude of the pulses can be reduced and PRR can be increased for high data rate short range applications. For low data rate long range applications, PRR can be decreased and pulses are made more powerful by increasing the amplitude [13].

Multipath immunity: Multipath is the phenomenon in which a wireless signal component undergoes scattering, reflection and refraction when it encounters obstructions like objects and surfaces in the communication channel. When the signal in radiated from transmitter antenna, some signal components undergo multipath propagation and becomes reflected

signal (non-line of sight propagation). As multipath signal components travelled through larger distances compared to direct signal (line of sight propagation) components, they arrive at the receiver with longer time of arrival (TOA). With every multipath distance varies, each multipath component's TOA depends on the path length, as shown in the Fig. 2.10. Each multipath component has different phase and undergoes severe distortion if two or more MPCs interfere with each other or with the direct signal components [2].

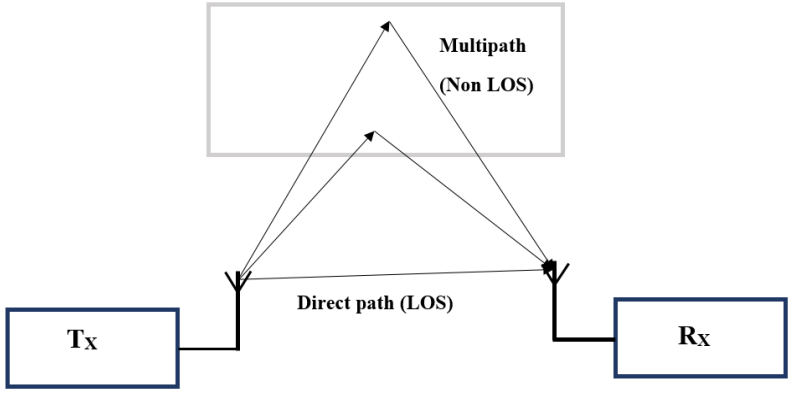

Figure 2.10: A multipath indoor wireless channel condition [2]

These multipath components can be resolved at the receiver, provided if they do not overlap with each other and can be distinguished from one another. In simple words, if two multipath components have enough separation in time, depending on the resolving power of the receiver, they can be resolved. As the pulse width decreases, separation between two multipath components will increase. This reduces the possibility of potential overlapping and destruction of two multipath components. As a result, using ultrashort pulses provide UWB systems robust immunity against multipath interferences while operating in a multipath environment.

Low operating power requirement: Very low EIRP emission limits on UWB signals makes it possible for an IR transceiver to operate with low power consumption. Ultrashort nature of the pulses, low duty cycle of the UWB signals and not using a carrier reduces the operating power requirement even more.

Simple transceiver architecture: An impulse radio transceiver architecture is relatively simple compared to traditional narrow band transceivers. Since impulse radio pulses are already in RF range, they can be transmitted through the medium without using a carrier signal, which eliminate the requirements of power amplifier, mixer and down conversion circuits in the transceiver. Hence, low developmental and operational costs can be achieved.

Low probability of interception: Low duty cycle and reduced emission levels make the interception and detection of IR signal difficult. This provides enhanced security to the wireless system [2].

Higher timing resolution: Due to the nature of ultrashort pulses, a UWB signal has high timing resolution, usually in the range of sub-nanoseconds. Ability to measure extremely small delays (sub-nanosecond delays) in the received signal makes it possible for the UWB receiver to analyze the transmitter position with the precision of few centimetres. This makes ranging and communication possible at the same time [2].

Finally, occupying several frequency bands gives IR UWB better penetrating properties, since signal penetrating properties vary significantly with frequency [2].

2.6 Applications of Ultra-wideband

Traditionally UWB technology was extensively used in military applications due to its signal properties. FCC in [1] classifies UWB systems into 3 main categories: (1) imaging systems, (2) vehicular radar systems and (3) communications and measurement systems. However, since the unregulated commercialization of UWB in 2002, many new commercial applications have been developed. Broadly both commercial and non-commercial applications of UWB can be classified into 3 categories [17]:

2.6.1 High Data Rate- Communication Applications

Communication uses of UWB mainly focus on short range (<10 m) and high data rate applications (up to 500 MBPS). Using UWB is ideal for high data rate, indoor point to point communications like: direct video streaming and connectivity between computer peripherals such as-wireless USB mouse, keyboard, printers and scanners. Some other examples include communication and data transfer between electronics devices like camera, audio system, portable video players and smart home appliances.

Due to the availability of massive bandwidth, data transfer rate of a UWB system can exceed most existing IEEE personal area network (PAN) and local area network (LAN) standards like Bluetooth (802.15.1), Zigbee (802.15.4) and Wi-Fi (802.11), as we can see from the Figure 2.11 [33]. 802.15.3a was a standardising committee established by IEEE to examine the possibility of using UWB as physical layer for high speed wireless personal area network (WPAN) [14].

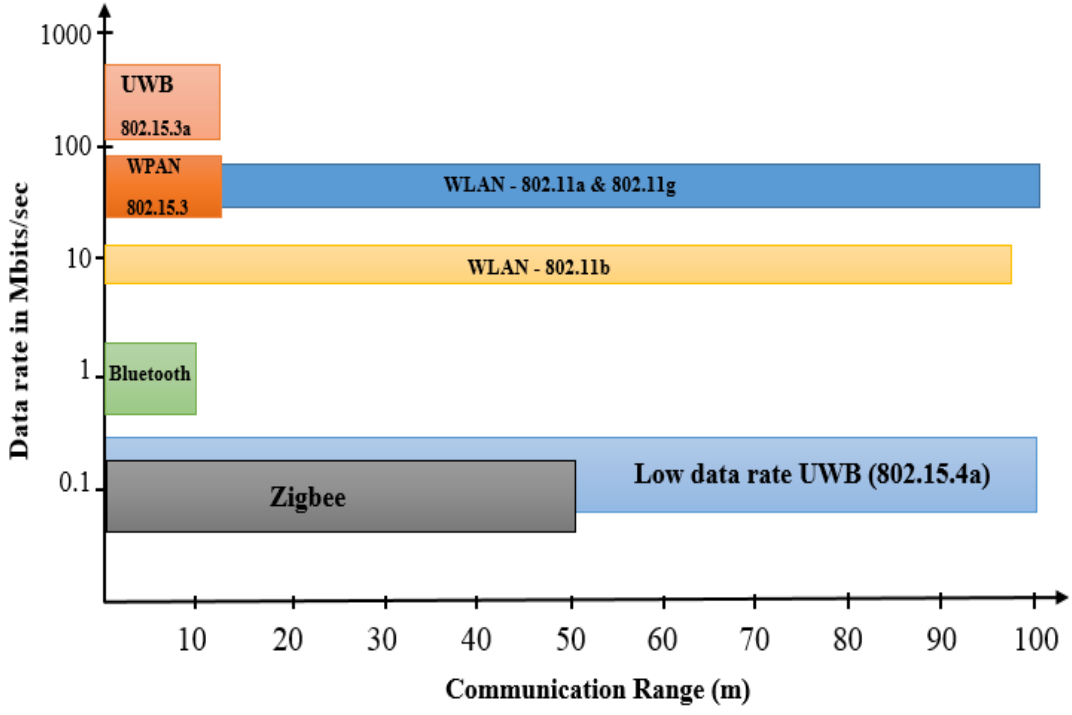

Figure 2.11: UWB vs other IEEE wireless standards

2.6.2 Low Data Rate- Positioning Applications

Low data rate UWB (please refer Figure 2.11) is widely used in positioning and tracking applications. Positioning generally needs large range (>10 m) but can function with low data rate (0.1-5 Mbps), so the emphasis is given to link distance. Using impulse radio provides very precise positioning (in the range of few centimeters) compared to sinusoidal signal. So low data rate IR UWB can find its application widely in sensor networks, industrial RF monitoring systems, object tracking, target positioning and intrusion detection. In healthcare, it can be used for patient monitoring and medical imaging purposes because of its low electromagnetic radiation level and precision capabilities.

2.6.3 Radar Applications

Being one of the original application, IR UWB is extensively used in both military and commercial radars. Better penetration properties, immunity for interception, resistance to jamming, accurate positioning capabilities and high resolutions make IR UWB ideal for radar applications [2]. Ground penetrating radars, collision avoidance systems in automobiles, altimetry, imaging radars and intelligent cruise control systems in vehicles can operate using IR UWB signals.

2.7 Challenges of IR UWB

Apart from wide range of advantages, IR UWB systems do face a few challenges. Main challenge is that wideband makes system design complex. Robust code synchronization algorithms with heavy processing requirements are needed at the receiver to achieve synchronization, particularly in multipath environments, if IR technology is used. Also, wideband circuit elements generally have higher power consumption and are more difficult to build than narrowband circuit elements. This makes the implementation of IR UWB system uneconomical, if carbon metal oxide semiconductor (CMOS) technology is used [18].

Low PSD and simple architecture involving IR pulses keep the transmitter design simple and energy efficient. However, received signal level at the receiver is normally very low, so the use of power amplifier becomes inevitable in practice. Additionally, coded ultrashort pulse train takes longer time to synchronize and causes overhead because of heavy processing requirements. These factors constitute to complex and power hungry receiver design requirements [34].

Main application target of UWB is short range, high data rate portable communication devices. These devices require smaller circuit designs and antennas, which can operate under varying channel conditions. Because of wide bandwidth and nonlinearity, designing a convenient antenna of small dimension becomes a problem [34].

Finally, very few UWB standardizing groups exist in IEEE. Apart from them, the UWB spectrum is heavily unregulated. This might result in potential interference between two UWB systems sharing the same frequency bands.

CHAPTER 3 IR UWB IMPLEMENTATION SCHEMES

Ultrashort pulses require complex synchronization and detection algorithms at the IR UWB receiver. This chapter reviews existing popular receiver implementations for impulse radio. Drawbacks of the exciting IR UWB receiver schemes, which led to the development of improved code shift reference schemes are also mentioned in this chapter. The code shift reference schemes on which the DCSR transceiver design is based are illustrated in subsequent sections. Finally, all mentioned impulse radio schemes are compared for performance.

3.1 Rake Receiver

As impulse radio signals are prone to multipath propagation, the received signal at the receiver consists of many multipath components (MPCs), particularly in NLOS channel environment [13]. Rake receiver is the most commonly used IR UWB receiver, which can effectively address the problem of multipath fading effect. Rake receiver collects the energy from all received resolvable multipath components of the signal and combines them. The original transmitted data is extracted from the combined energy of the all multipath components using a decision logic [13]. Figure 3.1 shows the structure of a commonly used Rake receiver.

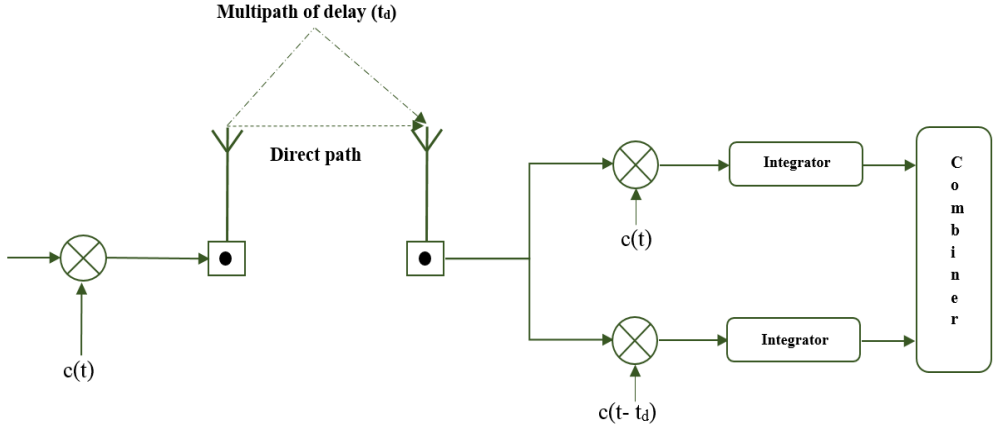

Figure 3.1: Structure of Rake receiver [35]

Each resolvable multipath signal component requires a "detecting finger" in the Rake receiver for its detection [13]. Since each MPC undergoes different kind of dispersion and distortion in the communication channel, in order to determine the amplitude, phase and delay of the MPC, each detecting finger needs continuous channel estimation, multipath acquisition and tracking operations. As the number of multipath components increase, the total number of detecting fingers required also increases. This ends up in the increased system complexity of the Rake receiver. If the number of detecting fingers (L) is equal to the number of resolvable MPCs in the signal, then the receiver is called coherent All Rake receiver (A Rake) and is shown in the Figure 3.2 [13].

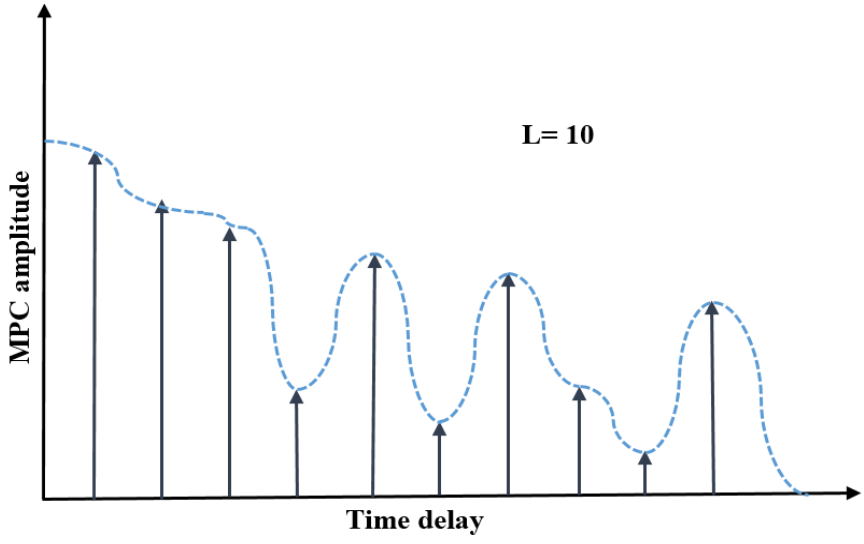

Figure 3.2: All Rake receiver [13]

To reduce the complexity of Rake receiver, the number of detecting fingers can be limited by selecting only few strongest MPCs in the signal, which is the operating principle of non-coherent Selective Rake receiver (S Rake), as shown in the Figure 3.3. Another way to limit the detecting fingers is, selecting only few first arriving MPCs at the receiver. This technique of MPCs selection based on the TOA is used in Partial Rake receiver (P Rake). However, the complexity reduction in both S and P Rake receiver has the disadvantage of performance degradation [13].

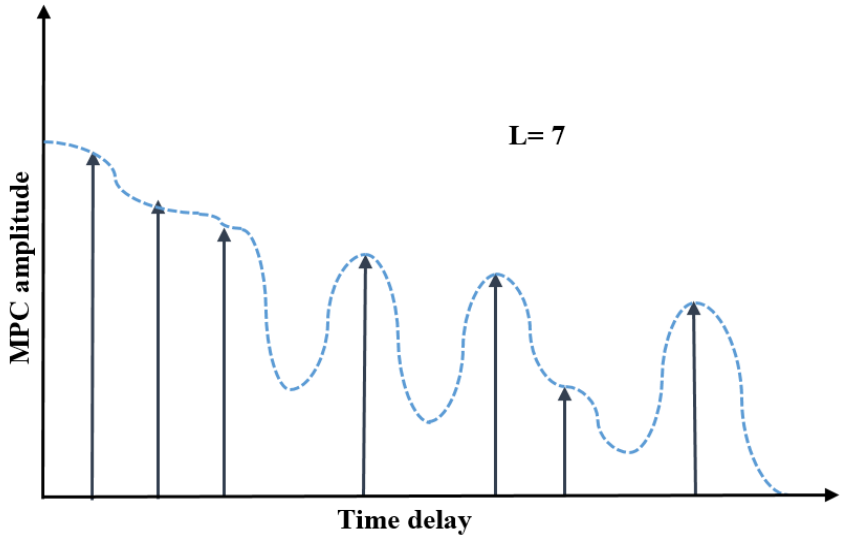

Figure 3.3: Selective Rake receiver [13]

3.2 Transmit Reference Scheme

To avoid the difficulties involved with channel estimation and multipath tracking, other coherent and non-coherent signaling schemes have been developed. One of such scheme is Transmit Reference (TR). To represent a data symbol (bit), convectional TR uses an unmodulated reference pulse and a data modulated pulse (doublet). While the reference pulse has a fixed polarity, data modulated pulse's polarity depends on the data bit [36]. Reference pulses and data modulated pulses are separated by time and the data modulated pulse is transmitted after reference pulse with a specific time delay of D. For this pair of time separated pulses (doublets) to use the same communication channel, the delay (D) between them should be less than the channel coherence time [33].

By propagating through the same channel, both reference and data modulated pulses undergo similar fading and distortions. At the receiver, received impulse radio signal component is correlated with its delayed version and is integrated to recover the original transmitted data [33]. General structure of transmit reference receiver is given in the Figure 3.4.

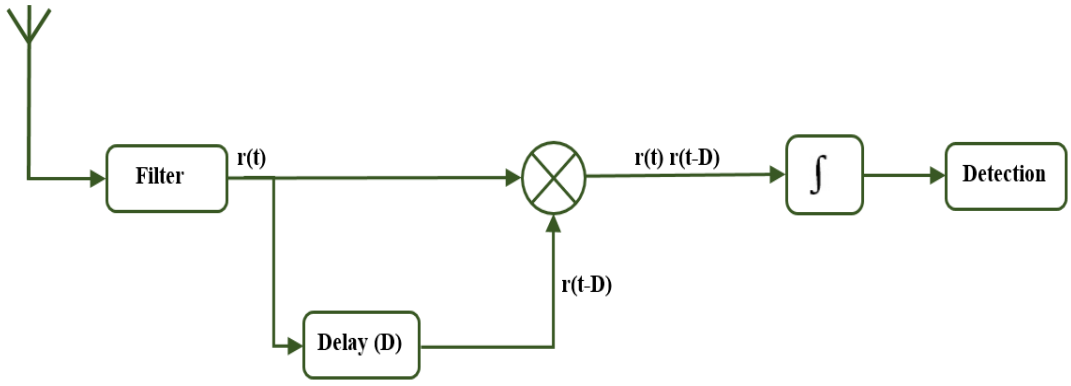

Figure 3.4: TR receiver structure [33]

Regardless of simplicity, TR has two primary disadvantages. Channel coherence time falls typically in the range of nanoseconds for IR UWB, so the delay elements need to be precise and should have the ability to handle wideband signals. However, realizing a wideband delay element with the accuracy in the order of nanoseconds is particularly difficult to achieve at circuit level [36]. Secondly, frequent overlapping of reference and data modulated pulses results in noise and the noise gets correlated at TR receiver as well, which causes performance degradation [10].

3.3 Frequency Shift Reference Scheme

To avoid the difficulties associated with the implementation of the delay element, TR scheme was further improved in [36], to develop Frequency Shift Reference (FSR) scheme. In FSR, reference pulses are shifted in frequency, such that they are orthogonal to data pulses over a symbol period. In simple words, reference and data modulated pulses are separated in frequency domain shifts. Frequency shift eliminates the necessity of time domain delay element. Since frequency translation is easier for wideband signals and is possible with a mixer, receiver implementation becomes simple if FSR is used. Simulations in [36] have also shown that FSR performs slightly better compared to TR in both AWGN and multipath channels.

One reference pulse can be used to transmit multiple data pulses simultaneously since each data pulse is shifted slightly using frequency shift. For both reference and data pulses to use the same channel for propagation, the frequency separation between them should be less than the channel coherence bandwidth. At receiver, the reference pulses are shifted again using the same offset frequency and data modulated pulses are integrated to extract the original transmitted bits [36]. Blocks of FSR receiver are shown in the Figure 3.5.

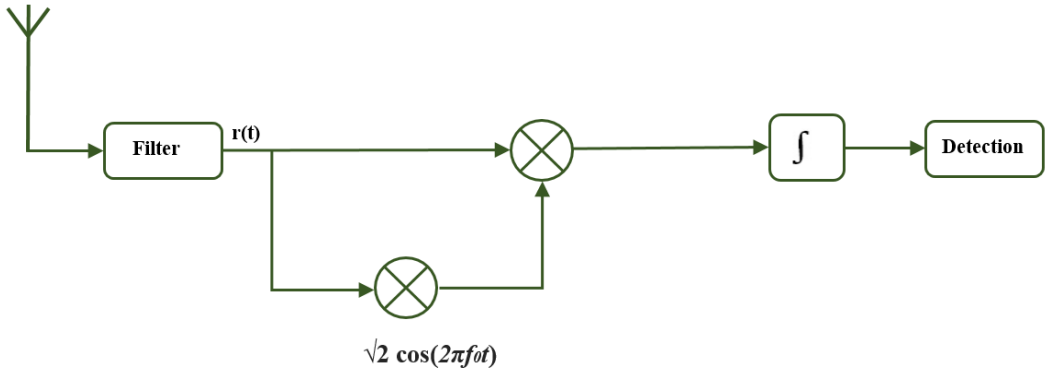

Figure 3.5: Structure of FSR receiver [36]

Using analog mixer and frequency conversion step makes FSR receiver power hungry. Also, FSR system suffers from volatile performance because of 1) frequency errors caused by analog oscillator which is used for frequency shift, 2) phase errors caused by multipath fading and 3) amplitude errors caused by nonlinearly of circuit elements respectively [3].

3.4 Code Shift Reference Scheme

If the separation of reference and data pulses is possible using time and frequency, it should be possible to separate them using specific shifting codes as well. Using this concept, to overcome the drawbacks and complexities involved with TR and FSR, a new scheme with better performance called Code Shift Reference (CSR) has been proposed in [3]. In all types of code shift reference schemes including CSR, data sequences are separated from reference sequences using specific shifting codes (such as Walsh codes). Simulation results in [5] show that the CSR scheme provides better performance compared to TR and

FSR. Absence of delay element and frequency shifting stage in CSR scheme keeps the transceiver architecture very simple.

3.4.1 CSR Transmitter Structure

Figure 3.6 shows the general structure of CSR transmitter [3].

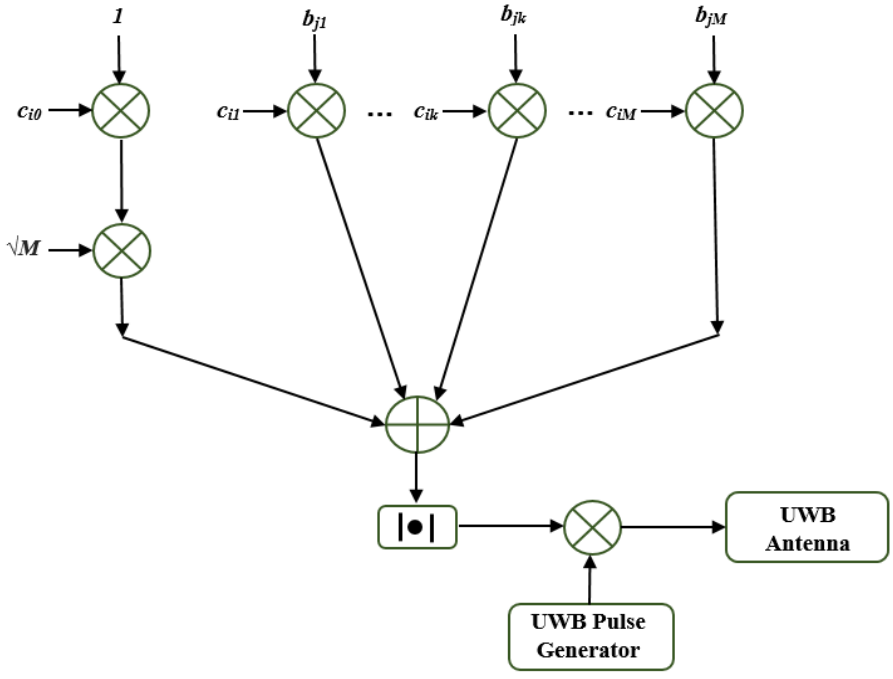

Figure 3.6: Structure of CSR UWB transmitter [3]

In CSR scheme, N_f frames are used to transmit M data bits at the same time [3]. The output of CSR transmitter can be expressed mathematically as:

$$x(t) = \sum_{j=-\infty}^{\infty} \sum_{i=0}^{N_f - 1} p[t - (jN_f + i)T_f] \left| \sqrt{M}\, c_{i0} + \sum_{k=1}^{M} b_{jk}\, c_{ik} \right| \tag{3.1}$$

in which, $p(t)$ is the duration (T_p) of UWB pulse, which covers the bandwidth of ($f_H - f_L$) in frequency domain; N_f is the number of frames used for the transmission of M bits; T_f is the time gap between two adjustment IR pulses in the pulse train; M is the number of

simultaneously transmitted information bits; $b_{jk} \in \{-1, +1)$ denotes the k^{th} information bit in the j^{th} N_fT_f time slot and $c_{ik} \in \{-1, +1\}$ is the shifting code for k^{th} information bit, which encodes the k^{th} bit into the pulse (i+1). Total number of shifting codes required for M bits is given by *(M+1)* [3]. The maximum M bits that can be transmitted simultaneously using $N_f = 2^N$ frames is limited to $M \leq 2^{N-1}$. The *(M+1)* shifting codes required to orthogonally separate the M data sequences from reference sequences is given below using the matrix, taken from [3]:

$$\begin{pmatrix} C_0 \\ \cdot \\ \cdot \\ \cdot \\ C_k \\ \cdot \\ \cdot \\ \cdot \\ C_M \end{pmatrix} == \begin{pmatrix} C_{00} & \cdots & C_{i0} & \cdots & C_{(Nf-1)\,0} \\ \cdot & & \cdot & & \cdot \\ \cdot & & \cdot & & \cdot \\ \cdot & & \cdot & & \cdot \\ C_{0k} & \cdots & C_{ik} & \cdots & C_{(Nf-1)\,k} \\ \cdot & & \cdot & & \cdot \\ \cdot & & \cdot & & \cdot \\ \cdot & & \cdot & & \cdot \\ C_{0M} & \cdots & C_{iM} & \cdots & C_{(Nf-1)\,M} \end{pmatrix} \tag{3.2}$$

3.4.2 CSR Receiver Structure

Structure of CSR UWB receiver is provided in the Figure 3.7, is taken from [3].

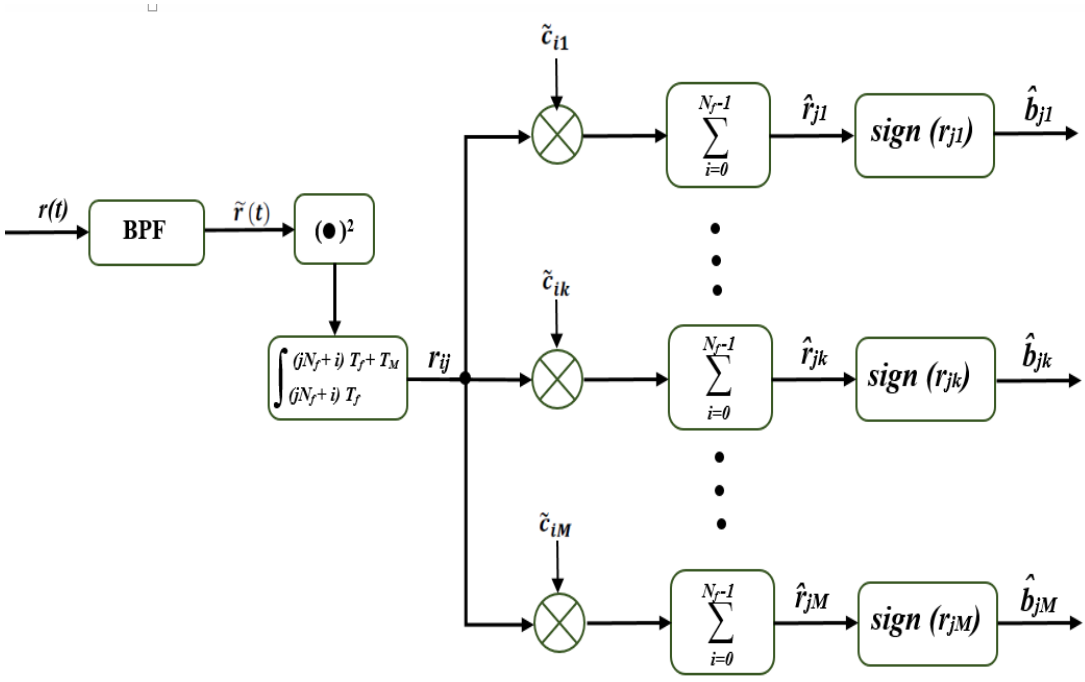

Figure 3.7: CSR UWB receiver structure [3]

The received CSR UWB signal is filtered using a band pass filter (BPF), which removes the noise and undesirable out of UWB band frequency components from the channel [3]. The signal is squared and integrated from $(jN_f+i)T_f$ th time to $\{(jN_f+i)T_f+T_M\}$ (T_p instead of T_M in AWGN channel and T_f in severe multipath channel) to calculate r_{ij}. Using M number of detection codes, r_{ij} is decoded to get the original transmitted information bit in the last stage [3]. The bit, either '0' or '1' is resolved by the sign of the correlator, after adding the detection code and r_{ij}, in each case [3]. The M detection codes are given in the form of matrix in equation 3.3, and are taken from [3].

$$\begin{bmatrix} \tilde{C}_0 \\ \vdots \\ \tilde{C}_k \\ \vdots \\ \tilde{C}_M \end{bmatrix} == \begin{pmatrix} \tilde{C}_{00} & \cdots & \tilde{C}_{i0} & \cdots & \tilde{C}_{(Nf-1)\,0} \\ \vdots & & \vdots & & \vdots \\ \tilde{C}_{0k} & \cdots & \tilde{C}_{ik} & \cdots & \tilde{C}_{(Nf-1)\,k} \\ \vdots & & \vdots & & \vdots \\ \tilde{C}_{0M} & \cdots & \tilde{C}_{iM} & \cdots & \tilde{C}_{(Nf-1)\,M} \end{pmatrix} \tag{3.3}$$

Shifting codes at the CSR transmitter and detection codes at the CSR receiver are selected from Walsh codes [3]. Table 3.1 provides Walsh codes as examples of CSR shifting and detection codes.

Code Length (N_f)	**Shifting Codes**	**Detection Codes**
$N_f = 2$	$c_0 = [1, 1]$ $c_1 = [1, -1]$	$\tilde{c}_1 = [1, -1]$
$N_f = 4$	$c_0 = [1, 1, 1, 1]$ $c_1 = [1, -1, 1, -1]$ $c_2 = [1, 1, -1, -1]$	$\tilde{c}_1 = [1, -1, 1 -1]$ $\tilde{c}_2 = [1, 1, -1, -1]$

Table 3.1: CSR shifting and detection codes [3]

3.5 Differential Code Shift Reference Scheme

Simulations in [5] show that CSR scheme performs better compared to TR and FSR schemes. However, in CSR scheme, half of the energy is used to transmit reference pulses. To transmit M bits simultaneously, CSR transmitter uses energy equivalent to (M/2) for the generation of reference pulses. To minimize this power consumption, CSR scheme was improved in [4] to develop Differential Code Shifted Reference (DCSR) scheme. DCSR is a novel scheme with better bit error rate performance compared to CSR, TR or FSR and uses only $[1/(M+1)]^{th}$ power in the form of reference pulses to transmit M data bits simultaneously. The power used by the transmitter to generate reference pulses decreases dramatically in DCSR, because DCSR scheme uses one pulse sequence as reference for another pulse sequence [4] [6].

3.5.1 DCSR Transmitter Structure

Structure of DCSR transmitter is shown in the Figure 3.8. As an improved version, DCSR system architecture is similar to CSR, except the information bits (d_{jk}) are differentially encoded [4].

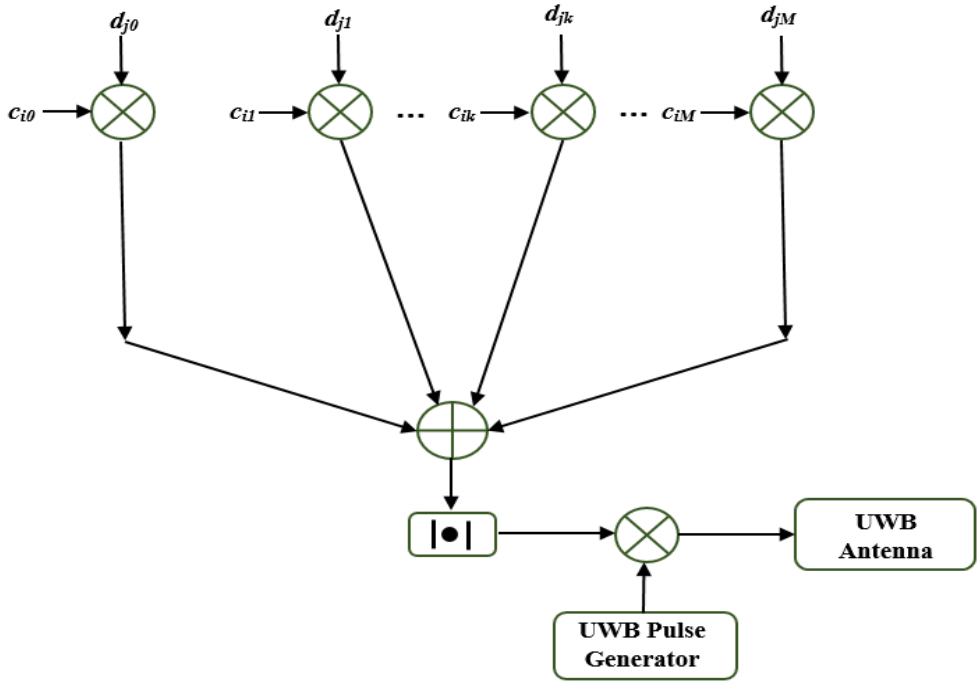

Figure 3.8: Structure of DCSR UWB transmitter [4]

Like in CSR, N_f pulse frames are needed to transmit M data bits. DCSR scheme can be mathematically represented as [4],

$$x(t) = \sum_{j=-\infty}^{\infty} \sum_{i=0}^{N_f - 1} p[t - (jN_f + i)T_f] \left| \sum_{k=0}^{M} d_{jk}\, c_{ik} \right| \tag{3.4}$$

in which, $p(t)$ is the pulse duration T_p; T_f being the frame duration; $c_{ik} \in \{-1, +1\}$ is the shifting code for k^{th} differential data bit d [4]. All DCSR signal notations represent the same parameters as that of CSR, given in the equation 3.1, except d_{jk}. $d_{jk} \in \{-1, +1\}$ is the differentially encoded bit transmitted in j^{th} N_fT_f period, given as:

$$d_{jk} = \begin{cases} 1 & k = 0 \\ \prod_{l=1}^{k} b_{jl} & \forall\ k \in \{1, 2, 3, 4 \ldots M\} \end{cases} \tag{3.5}$$

The $(M+1)$ shifting codes used to encode and transmit simultaneous M bits in DCSR are same as that of CSR, already expressed in the form of matrix in the equation 3.2 [4]. The DCSR transmits $[M\ (M+1)/2] \leq 2^N - 1$ information bits per N_f frames, where $N_f = 2^N$.

3.5.2 DCSR Receiver Structure

Due to the differential encoding of data bits, DCSR receiver architecture differs slightly from that of CSR receiver. Blocks of DCSR receiver are given in the Figure 3.9 [4].

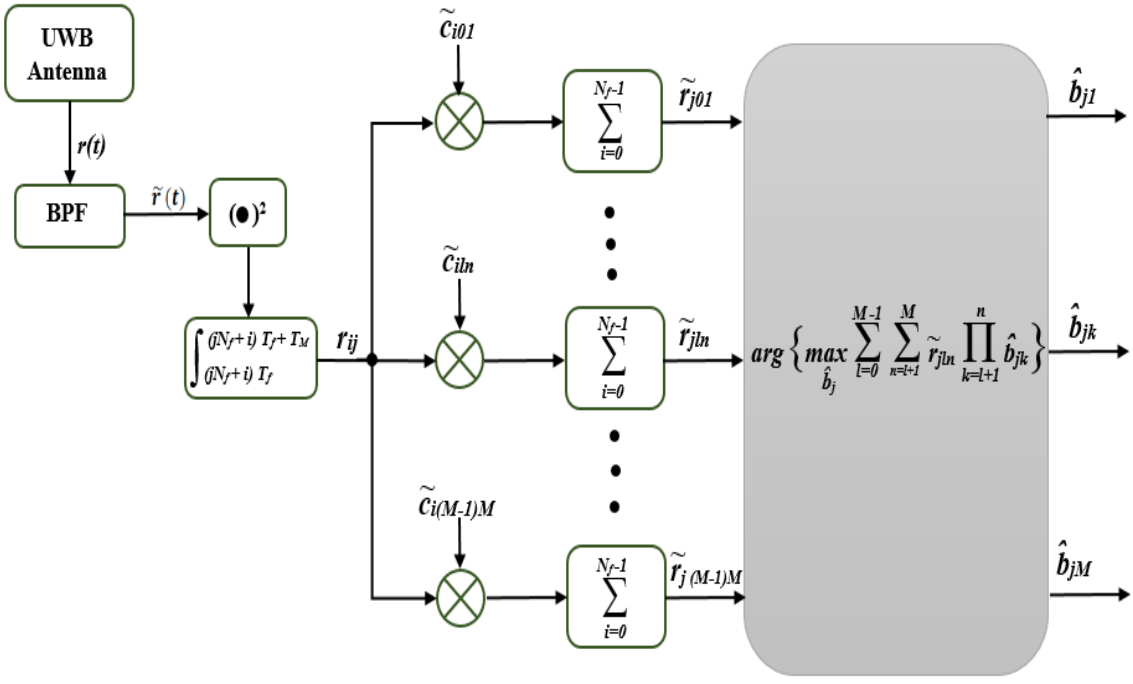

Figure 3.9: DCSR UWB receiver structure [4]

The received signal is band pass filtered and squared in the first stage [4]. Then the signal is integrated from $(jN_f + i)T_f$ th time to $[(jN_f + i)T_f + T_M]$ to obtain r_{ij}. The obtained r_{ij} is correlated with $[M\ (M+1)/2]$ detection codes, to obtain $\tilde{r}_{jln,}$ where, $\{l \in 0, 1, 2 \ldots\ (M -$

1)} and *{n ∈ (l+1), (l+2), (l+3)……M}*. The decision rule given in the equation 3.6 is applied to $\tilde{r}_{jln}$ in each case, which extracts the original transmitted data bit [4].

$$\hat{b}_j = arg\left\{ \max_{\hat{b}_j} \sum_{l=0}^{M-1} \sum_{n=l+1}^{M} \tilde{r}_{jln} \prod_{k=l+1}^{n} \hat{b}_{jk} \right\} \tag{3.6}$$

The DCSR [*M (M+1)/2*] detection codes are expressed using the matrix method in the equation 3.7 [4].

$$\begin{pmatrix} \tilde{C}_{01} \\ \vdots \\ \tilde{C}_{0M} \\ \tilde{C}_{12} \\ \vdots \\ \tilde{C}_{1M} \\ \tilde{C}_{23} \\ \vdots \\ \tilde{C}_{(M-1)M} \end{pmatrix} = \begin{pmatrix} \tilde{C}_{001} & \cdots & \tilde{C}_{i01} & \cdots & \tilde{C}_{(Nf-1)01} \\ \vdots & & \vdots & & \vdots \\ \tilde{C}_{00M} & \cdots & \tilde{C}_{i0M} & \cdots & \tilde{C}_{(Nf-1)0M} \\ \tilde{C}_{012} & \cdots & \tilde{C}_{i12} & \cdots & \tilde{C}_{(Nf-1)12} \\ \vdots & & \vdots & & \vdots \\ \tilde{C}_{01M} & \cdots & \tilde{C}_{i1M} & \cdots & \tilde{C}_{(Nf-1)1M} \\ \tilde{C}_{023} & \cdots & \tilde{C}_{i23} & \cdots & \tilde{C}_{(Nf-1)23} \\ \vdots & & \vdots & & \vdots \\ \tilde{C}_{0(M-1)M} & \cdots & \tilde{C}_{i(M-1)M} & \cdots & \tilde{C}_{(Nf-1)\,(M-1)M} \end{pmatrix} \tag{3.7}$$

Like in CSR, transmitter shifting codes and receiver detection codes are obtained from Walsh codes for DCSR [4].

Code Length (N_f)	Shifting Codes	Detection Codes
$N_f = 2$	$c_0 = [1, 1]$ $c_1 = [1, -1]$	$\tilde{c}_{01} = [1, -1]$
$N_f = 4$	$c_0 = [1, 1, 1, 1]$ $c_1 = [1, -1, 1, -1]$ $c_2 = [1, 1, -1, -1]$	$\tilde{c}_{01} = [1, -1, 1 -1]$ $\tilde{c}_{02} = [1, 1, -1, -1]$ $\tilde{c}_{12} = [1, -1, -1, 1]$

Table 3.2: DCSR shifting and detection codes [4]

3.6 DCSR Encoding: An Example

1). The DCSR prototype transceiver developed by our research group works using four frames (N_f =4) at the moment. As $N_f = 2^N$, the number of bits that can be transmitted simultaneously is given by $[M(M+1)/2] \leq 2^N - 1$, where N=2. This gives $M = 2$.

2). For M =2, number of orthogonal shifting codes required is $(M+1)$ = 3. The shifting codes are taken from the table 3.2: $c_0 = [1, 1, 1, 1]$; $c_1 = [1, -1, 1, -1]$; $c_2 = [1, 1, -1, -1]$;

3). **Differential encoding**: Consider two simultaneously transmitting M data bits "10". $b_{j1} = 1$, $b_{j2} = 0$. Therefore, $d_{j0} = 1$ (d_{j0} value is fixed); $d_{j1} = b_{j1} = 1$; $dj_2 = b_{j1} * b_{j2} = 0$;

4). **Bipolar expression**: In bipolar expression '1' represented by '+1' and '0' by '-1'.Thus, differentially encoded data bits become:

$d_{j0} = +1$; $d_{j1} = +1$; $dj_2 = -1$;

5) **Code shift**: Differentially encoded data bits undergo code shift modulation when they are multiplied with orthogonal shifting codes. Now they become DCSR modulated pulses.

$d_{j0} * c_0 = [1, 1, 1, 1]$

$d_{j1} * c_1 = [1, -1, 1, -1]$

$d_{j2} * c_2 = [-1, -1, 1, 1]$

$|\bigoplus| \Rightarrow | [1, -1, 3, 1] | \Rightarrow [1, 1, 3, 1]$,

where, pulse '3' has 3 times the amplitude of pulse '1'. All four possible pulse combinations, when N_f=4 and M =2, after DCSR modulation are given in the Table 3.3.

b_1b_2	DCSR output
00	1 3 1 1
01	1 1 1 3
10	1 1 3 1
11	3 1 1 1

Table 3.3: All possible DCSR encoding patterns, when $N_f = 4$

3.7 Performance Comparisons between IR Schemes

All the existing popular IR UWB schemes mentioned in this chapter were compared for bit error rate (BER) performances using SNR level as the parameter in [5] and [6]. Because of the digital implementation of shifting codes, both CSR and DCSR were able to perform

better compared to TR and FSR. TR and FSR suffer from performance degradations because of the use of analog delay element and frequency mixer. Bit error rate performance simulations were carried out without considering the effects of inter-pulse interference. In each case, it was assumed that there are no inter symbol interferences (ISI) between the pulses of the signal.

Bit error rate of CSR is given by [5],

$$BER_{CSR} = Q\left(\frac{\sqrt{M}\ \alpha E_b}{\sqrt{2M\alpha E_b N_0 + N_0^2\ (f_H - f_L) N_f}\ T_M} \right) \tag{3.8}$$

where, M is the number of simultaneously transmitted information bits; $\alpha \in (0, 1)$ (α=0, when T_m=0; and α=1, for T_M=T_f); E_b is the energy per received information bit; N_0 is the AWGN channel's single side power spectral density; $(f_H - f_L)$ is the bandwidth of the signal; N_f is the number of frames transmitted; T_m is the receiver integration time (T_m varies to T_p in AWGN channel and T_f in severe multipath channel) [5].

To verify the theoretical BER of CSR transceiver obtained from the equation 3.8, Monte Carlo simulations were carried out using the IEEE 802.15.4a channel model for the multiple values of M and N_f. The simulations were carried out using T_f= T_M= 60ns (α=1). As it can be seen from the Figure 3.10, BER improves with the increase in M and/or E_b/N_0. Also, simulation results match accurately with theoretical results [5].

Similarly, computer simulations were done for the DCSR scheme in [6] to compare the BER with theoretical results using T_f=T_M=60ns (α=1). Like in CSR, BER of DCSR system improves with the increase of M, (M/N_f) and (E_b/N_0). Simulation results are provided in the Figure 3.11. BER of DCSR is given by [5],

$$BER_{DCSR} < 2Q\left(\sqrt{\frac{32\ (\alpha E_b)^2}{60\alpha E_b N_0 + 9N_f N_0^2\ (f_H - f_L) T_M}} \right), \quad for\ M=2 \tag{3.9}$$

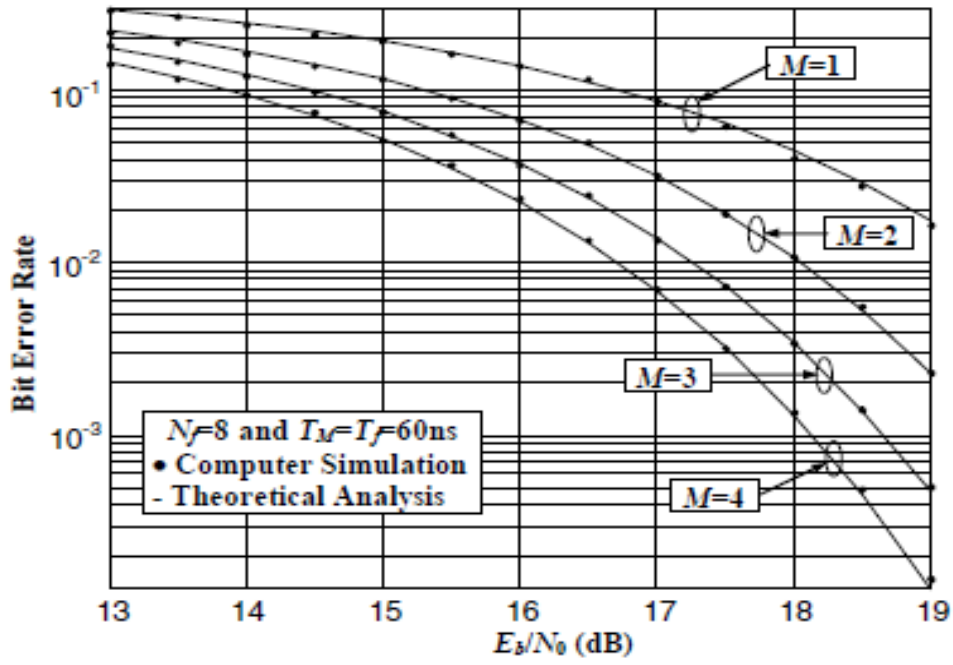

Figure 3.10: Theoretical vs simulation BER analysis for CSR UWB System [5]

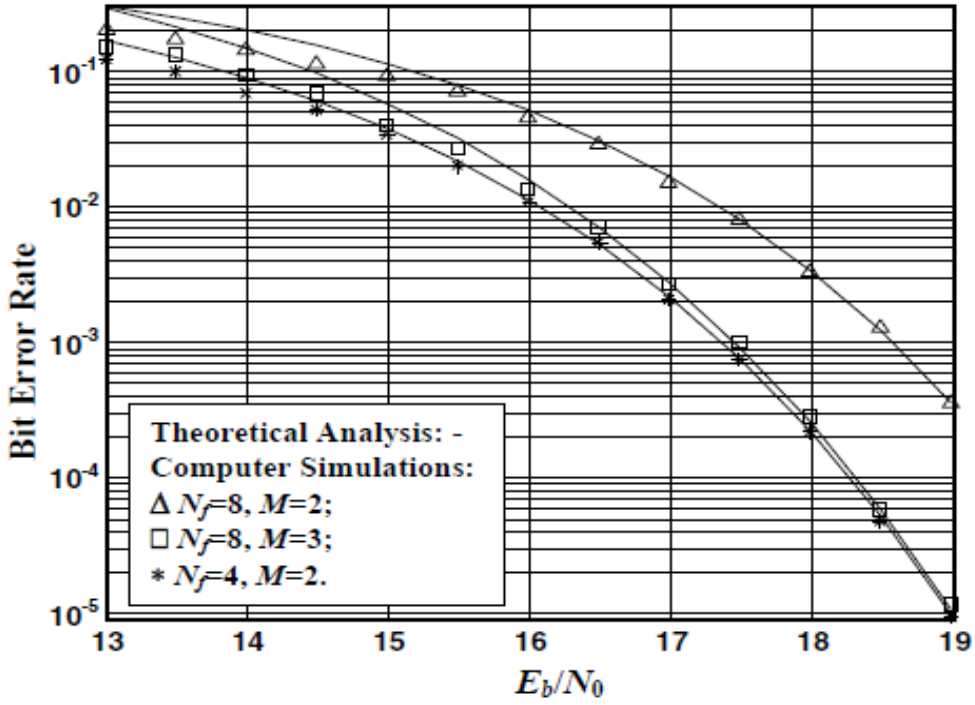

Figure 3.11: Theoretical vs simulation BER analysis for DCSR UWB System [6]

TR and FSR were compared with CSR and DCSR for the BER performance using simulations, when M=2 and M=3. For the transmission of M simultaneous bits, N_f value for each scheme is different since the minimum N_f requirement varies among the schemes. Multipath channel conditions with no inter pulse interference scenarios were used for the BER performance simulations of TR, CSR and DCSR, since no multipath phase errors exist in these schemes. However, BER performance was simulated using AWGN channel for FSR, as its performance degrades even more in a multipath channel [6]. This phenomenon is due to the use of analog carriers in FSR, which are prone to phase errors in a multipath channel. Figures 3.12 and Figure 3.13 show the BER performance comparisons between TR, FSR, CSR and DCSR for M=2 and M=3, respectively [6].

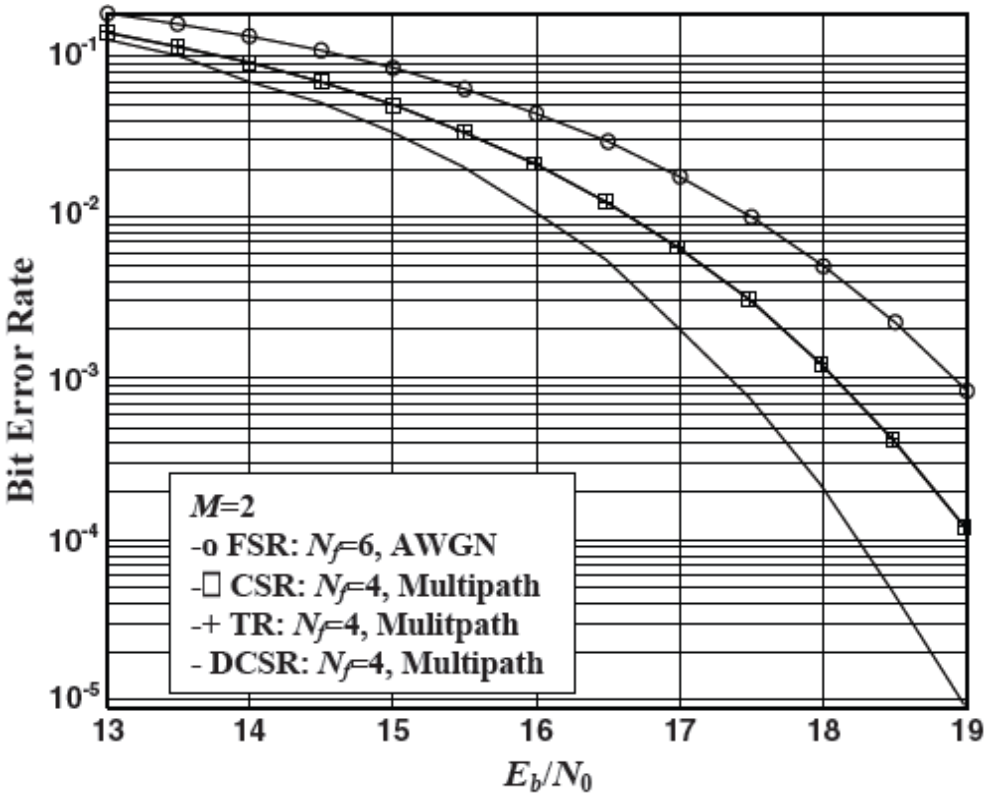

Figure 3.12: BER performance simulations for TR, FSR, CSR and DCSR, when M=2 [6]

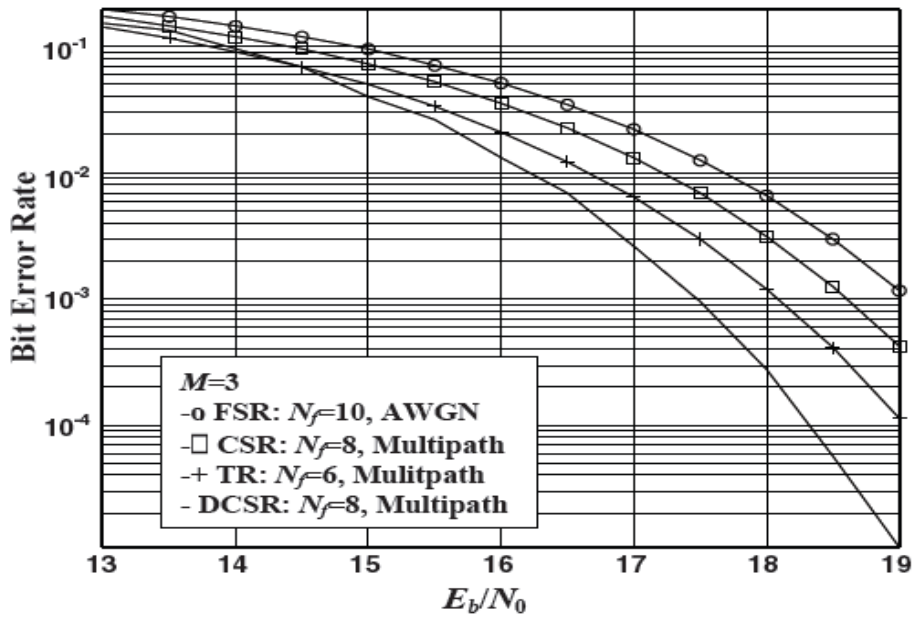

Figure 3.13: BER performance simulations for TR, FSR, CSR and DCSR, when M=3 [6]

As can be seen from the plots, apart from high SNR, BER performance improves in two scenarios: a) with the increase in bit to frame ratio (M/N_f) and b) reduction in the power used by the system for the transmission of reference pulses. Among four compared IR UWB schemes, best performance was achieved by DCSR, in both the cases of M=2 and M=3 [6]. Obtained performance results are elaborated below.

a) **When M=2**: FSR gives the worst performance because of the lowest bit to frame (M/N_f) ratio. TR and CSR provide similar performances not only because of the same M/N_f ratio, but also because of the same amount of power consumption for the generation of reference pulses (1/2 of the total power). Though M/N_f ratio is same for TR, CSR and DCSR, best performance is provided by DCSR. This is possible because, ½ the power of the TR and CSR transmitters are used to transmit the reference pulses. Whereas, only $1/(M+1)^{th}$ transmitter power is used by the reference pulses in DCSR [6].

b) **When M=3:** In this case also FSR has the lowest (M/N_f) ratio and uses half the power to transmit reference pulses. These factors make the performance of FSR poorest when it is compared with other IR UWB schemes. Performance of TR improves compared to CSR because of the improvement in (M/N_f) ratio. DCSR still offers the best performance since

the total power consumed by the transmitter for the transmission of reference pulses is low (*1/ (M+1)*) and decreases compared to TR and CSR [6].

Table 3.4 clearly illustrates the advantages of DCSR compared to other IR UWB schemes. The original chart was provided in [6] and it also compares all the main features of the popular IR UWB systems mentioned in this chapter.

	TR	**FSR**	**CSR**	**DCSR**
Delay Element	Yes	No	No	No
Analog Carrier	No	Yes	No	No
Shifting Codes	No	No	Yes	**Yes**
Multipath Errors	No	Yes	No	No
Reference Power	1/2	1/2	1/2	**1/(*M*+1)**
PAPR	Low	High	Medium	Medium
M/N_f	1/2	< 1/2	maximum 1/2	maximum 1/2
Complexity	High	High	Low	Low
Performance	Good	Poor	Good	**Best**

Table 3.4: Comparisons between TR, FSR, CSR and DCSR [6]

CHAPTER 4 DCSR UWB TRANSCEIVER STRUCTURE

This chapter provides the architecture and describes the basic functional blocks of DCSR IR UWB transceiver which is currently under development. The circuit level modifications done at the pulse amplitude modulation stage of the transmitter to get the desired pulse ratio are presented in this chapter.

4.1 DCSR Transmitter

DCSR transmitter block diagram is shown in the Figure 4.1

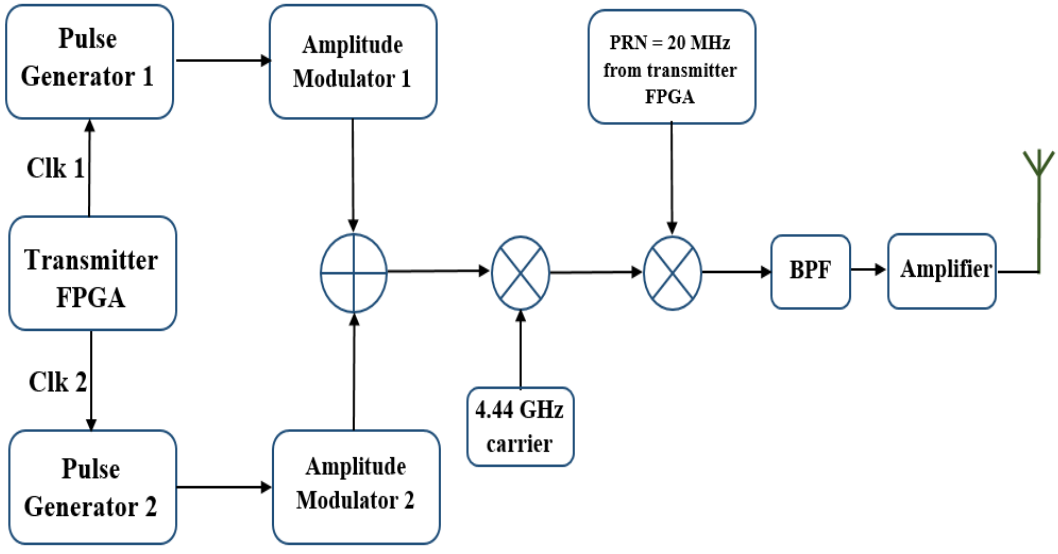

Figure 4.1: DCSR transmitter structure

In the first stage, DCSR data modulated clocks are digitally generated in the transmitter FPGA. Data sequence from MAC layer is digitally modulated according to DCSR encoding algorithms as described in [4] inside FPGA. Since the MAC layer is not yet developed for the DCSR system, a test sequence is used to generate DCSR data modulated clocks for existing transmitter [7]. For example**,** when two simultaneous bits "11" undergo DCSR modulation (for our system *M=2*), they become DCSR data modulated pulse sequence of "3111", where pulse '3' amplitude is three times the actual amplitude of pulse

'1' (this pulse amplitude modulation of 3:1 occurs in later stages). Transmitter FPGA is programmed to generate two separate 20 MHz clocks of same amplitude using On-Off keying to produce pulse '3' and pulse '1' sequences. When there is pulse '3', Clock_2 is triggered and Clock_1 is off and vice versa [7] [8]. Figure 4.2 shows the generated DCSR data modulated clocks in FPGA.

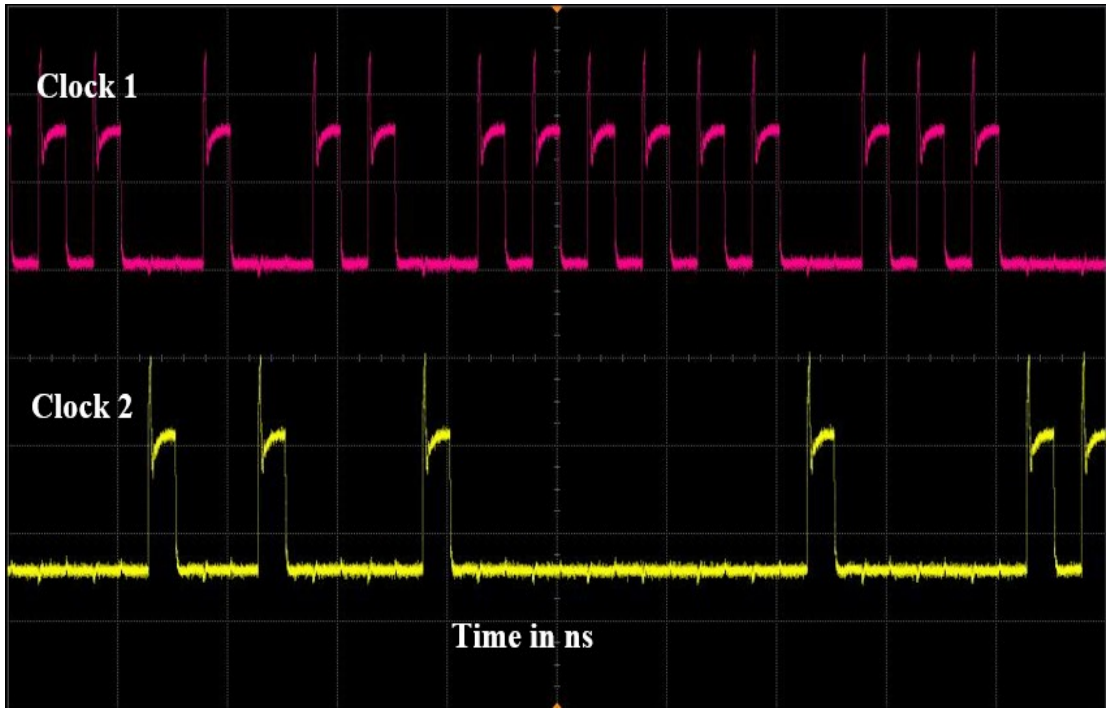

Figure 4.2: DCSR data modulated clocks from FPGA [7] [8]

In the next step, both data modulated clocks from FPGA are fed to pulse generator circuits. There are two identical pulse generators-each for a clock sequence from FPGA. Pulse generators shape the received FPGA clocks to IR UWB pulses, such that the frequency spectrum of those pulses meet the FCC defined bandwidth requirements of commercial UWB. As already discussed in chapter 2, energy efficiency of the UWB transmitter is closely related to the pulse shape. Therefore, curve functions like Gaussian pulse and its derivatives are typically used during the generation of UWB pulses. Each Pulse of DCSR UWB system is generated using the Gaussian pulse function at present. The delay elements, inverters and high speed on-off switching transistors used in the pulse generator circuits' approximate the rectangular data modulated clocks from FPGA to Gaussian

pulses [8]. Each generated Gaussian pulse has the duration of 4 ns, creating 500 MHz signal, as bandwidth is inversely proportional to pulse duration. Outputs of both pulse generators are shown in Figure 4.3.

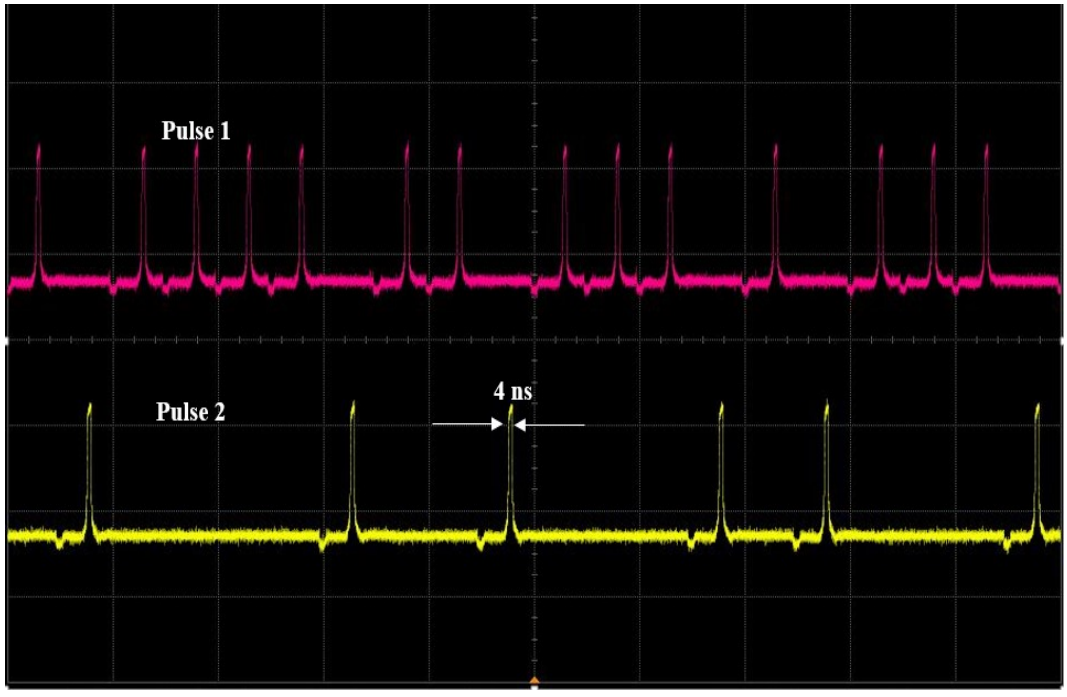

Figure 4.3: DCSR pulse generators outputs [8]

Next stage is pulse amplitude modulation and pulse combining. The pulse amplitude modulation (PAM) stage consists of two inverting Op Amps with the gain ratio of 3:1. The pulse sequence '2' from pulse generator 2, which was originally generated from Clock_2 of FPGA is given to the Op Amp with gain '3' to become pulse '3'. The pulse sequence '1' from pulse generator 1, which was generated from Clock_1 is given to Op Amp with gain '1' and becomes pulse '1' [8]. Thus, DCSR data modulated pulses undergo pulse amplitude modulation to become actual pulse sequences of the ratio of 3:1 in this stage. Then both the pulse sequences are combined to form a single pulse train. In the next step, the DCSR pulse train is mixed with a carrier signal of 4.44 GHz using RF mixer [8]. This carrier up conversion moves the DCSR IR UWB spectrum to 4.44 GHz ± 250 MHz band, a part of radio spectrum unlicensed by FCC for UWB commercial applications.

Frequency spectrum of DCSR UWB signal after RF mixing stage shows a sequence of spectral lines which are more powerful by 12 dB than rest of DCSR spectrum [9]. These spectral lines repeat throughout the bandwidth of UWB signal at every 20 MHz. These interfering lines are caused by the baseband data pulses which repeat in every 20 MHz interval. As the lines exceed FCC UWB emission mask, significant signal power reduction is necessary to eliminate them from the signal spectrum, which results in transmitter performance degradation.

One of the methods to remove these spectral lines without degrading the transmitter performance is to spread the energy in these lines evenly throughout the entire signal bandwidth [9]. A pulse polarity modulator was implemented in [9] to generate a pseudo random number sequence (PRN) using a 15 bit linear feedback shift register (LFSR) and is placed at the end of transmitter. The digital LFSR implemented in FPGA generates a random sequence of length $2^n - 1$ (in this case, n=4). The polarity modulated PRN sequence (in ±180º phase) is mixed with DCSR UWB signal (has the effect multiplying the signal by ±1), which eliminates the energy in unwanted spectral lines. At the receiver, received signal is squared and squaring cancels the polarity modulation effects on DCSR signal [9].

The DCSR UWB signal is then band limited to 500 MHz using a band pass filter. The signal bandwidth is ±250 MHz with the center frequency of 4.4 GHz. Then the signal is amplified using a power amplifier and radiated to the wireless communication channel using an impulse radio UWB antenna.

4.2 DCSR Receiver

DCSR receiver has 3 main stages [7] [8]. Signal recovery is the first stage which filters the noise and interferences from the communication channel. This stage also amplifies the received signal to a suitable level for future detection. The second is the high frequency removal stage in which the signal is squared and down-converted to its baseband by removing the carrier. In the following synchronization & detection stage, the baseband

signal undergoes timing recovery and is sampled for future detection. Finally, the sampled signal is decoded in the decoding stage. The decoding stage operates in FPGA. All three main blocks of the DCSR receiver are provided in the Figure 4.4 [7] [8] [10] [11].

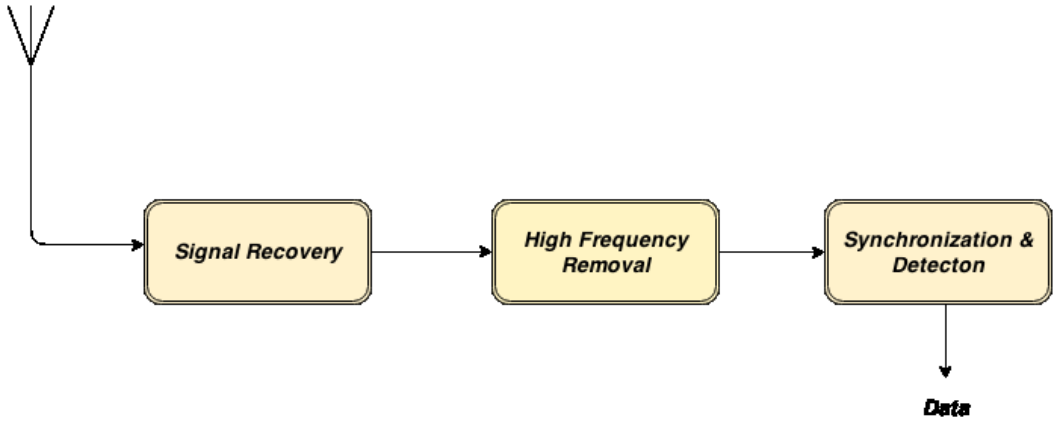

Figure 4.4: Main blocks of DCSR receiver [7] [8] [10] [11]

Signal recovery: This block consists of a band pass filter (BPF), a wideband low noise amplifier (LNA) and an automatic gain control (AGC) unit. The BPF filters out the noise and interference components in the DCSR UWB signal, which were induced in the channel. The LNA and AGC adjust the amplitude of the received signal to a constant desired level for further processing.

The core of feedback RF AGC is a variable gain amplifier (VGA). The gain of VGA is controlled by a digital control signal. Normally the durations of the distortions induced in the signal by the communication channel are much longer than the duration of DCSR IR UWB pulses. So DCSR pulses are treated as high frequency components and the disturbances from the varying communication channel are treated as the low frequency components. Therefore, a VGA control signal generation algorithm based on the idea of low pass filter (LPF) is presented in [12] and implemented using AGC unit. The function of the algorithm can be described as averaging the high '3' and the low '1' pulses of the received DCSR signal, i.e. smoothing effect. The parallel digital control signal for VGA from receiver FPGA is generated as follows [12]:

- If the received DCSR signal strength in receiver FPGA is less than that of reference signal ($V_{ref} > V_{received}$), the control signal generation algorithm in FPGA sends a stronger control signal to VGA, which increases the VGA gain, such that received and reference signal strengths can be balanced.

- If the received signal strength at the receiver FPGA is higher than that of the reference signal strength ($V_{ref} < V_{received}$), a weaker control signal is sent to VGA, decreasing the VGA gain, so that actual and reference signal strengths are balanced.

- If received signal strength at FPGA is same as that of the reference signal ($V_{ref} = V_{received}$), gain is kept same.

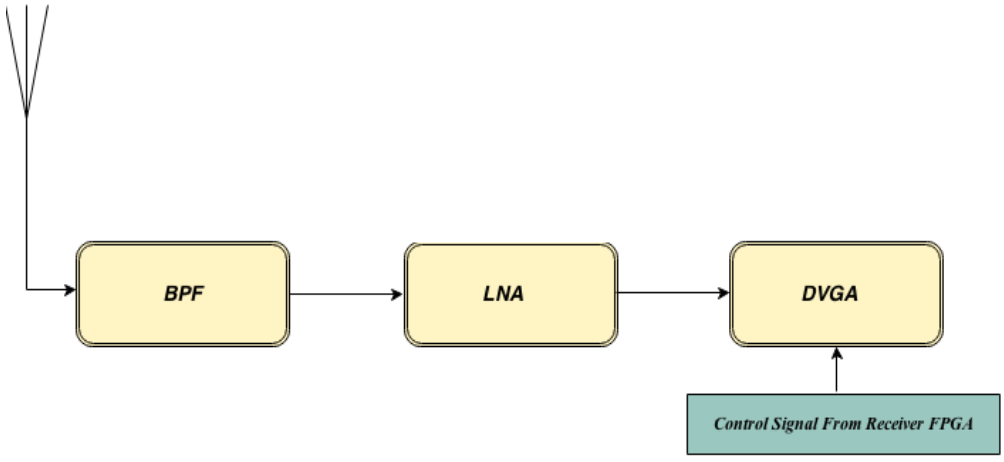

Figure 4.5: Signal recovery stage [8] [12]

High frequency removal: In this stage, as shown in the Figure 4.6, DCSR RF signal is squared. The signal from the signal recovery stage is split using a power splitter and combined again using a mixer, which results in squaring effect on the signal. After squaring, the pre-existed pulse ratio of 3:1 between high and low pulses increases to 9:1.

A low pass filter removes the carrier signal frequency components at 4.44 GHz, leaving only the baseband pulses. The signal is then amplified again and given to energy detection block [8].

Figure 4.6: High frequency removal stage [7] [8]

Detection and decoding: Blocks in this stage are shown in the Figure 4.7. This stage consists of a voltage buffer, active low pass filter (active LPF), an analog to digital converter (ADC) and a phase locked loop (PLL) incorporated with receiver FPGA [10] [11].

A DC voltage buffer offsets the DC that gets injected when the multiplier at the squaring stage shifts a signal component of the DCSR RF spectrum to DC range. The main function of the detection stage is to synchronize the clock of the receiver with the transmitter clock and to sample the received DCSR data modulated pulses for the next stage to extract the original data bits. An active LPF widens the narrow 4 ns DCSR pulses to 35 ns pulses for signal energy detection purpose. These expanded pulses are sampled by ADC using 80 MHz sampling clock, which is generated by VCXO in the receiver FPGA [10]. Briefly, the ADC oversamples the widened pulses by 4x rate. The readings from the ADC sampling allow the FPGA to detect the phase difference between local receiver clock and the clock of the transmitter. FPGA generates a control signal using the algorithms mentioned in [10]. Using the control signal, the PLL feedback loop synchronizes and locks the receiver clock with the transmitter clock by increasing or decreasing receiver clock frequency.

Once both transmitter and receiver clocks are synchronized for the non-coherent detection of data**,** decoding of the DCSR data modulated pulses occur in receiver FPGA to extract the original data bits. 'Direct searching' symbol synchronization and bit detection algorithm is demonstrated in [37] and is digitally implemented in receiver FPGA. This algorithm is presently being used for decoding purposes.

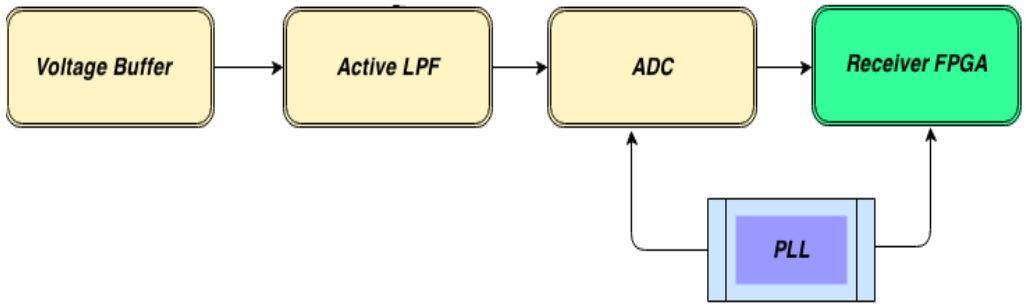

Figure 4.7: Detection and decoding stage [10] [11]

4.3 Nonlinearity of Transmitter RF Mixer

When moving from simulations to the implementation of the DCSR transmitter, use of the mixer circuit to inject 4.44 GHz carrier signal to the baseband DCSR pulses created a challenge. As previously mentioned, inverting Op Amps are used in the pulse amplitude modulation stage. Gains of the Op Amps play the key role in the amplitude modulation of two identical DCSR pulse trains to obtain the desired pulse ratio of 3:1 between them. The gain of an Op Amp is given in the equation 4.1.

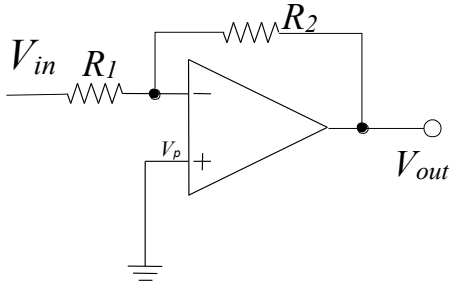

Figure 4.8: Structure of inverting Op Amp

$$V_{out} = -\left(\frac{R_2}{R_1}\right)V_{in} \tag{4.1}$$

Therefore, to generate pulse '1' sequence, the ratio (R_2/R_1) of the Op Amp 1 was kept equal to 1 by using the 1kΩ resistors for R_2 and R_1 in [8]. To generate the pulse '3' sequence,

(R_2/R_1) ratio of Op Amp 2 was maintained to 3 by using R_2=3 kΩ and R_1=1 kΩ. The Agilent ADS schematic circuit of the pulse amplitude modulation stage used for simulation in [8], is provided in the Figure 4.9 and the simulation result is provided in the Figure 4.10 [8].

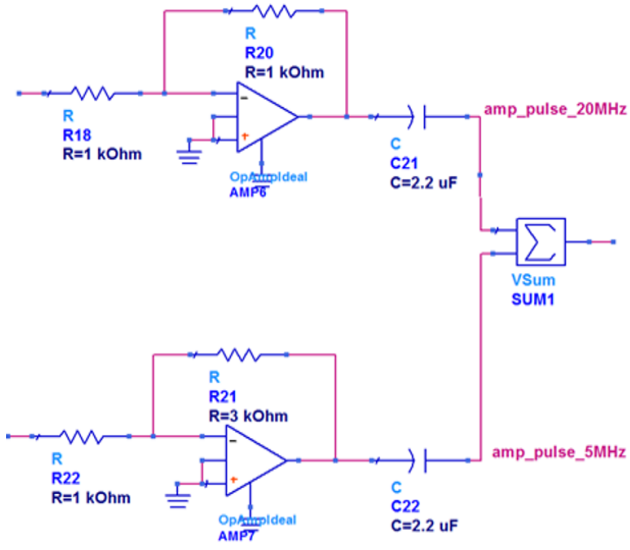

Figure 4.9: Pulse amplitude modulation circuit using ADS [8]

As shown in the Figure 4.10, the ratio between the high pulses '3' and low pulses '1' is 3:1. The ratio stays same in the simulation results even after the gated pulse stage, where 4.44 GHz carrier is mixed with the baseband pulses, as seen the Figure 4.11. This is due to non-linear factors of wideband mixer circuit elements were not taken into consideration by ADS electronic design automation software during the simulations [8].

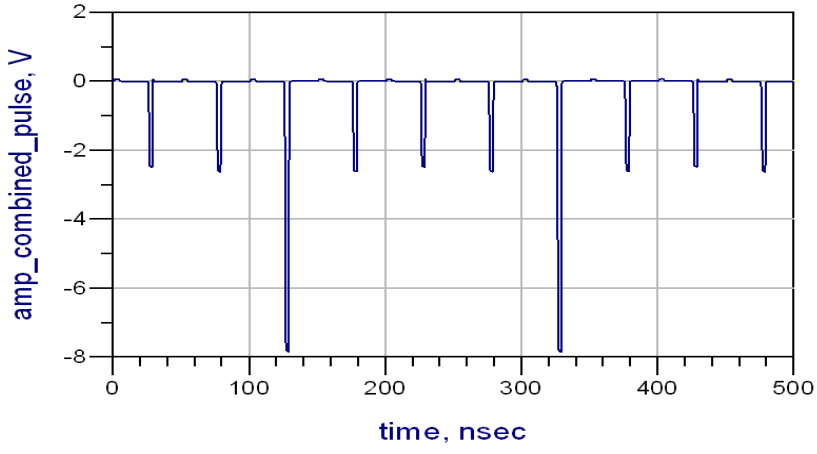

Figure 4.10: Pulse amplitude modulation stage simulation output [8]

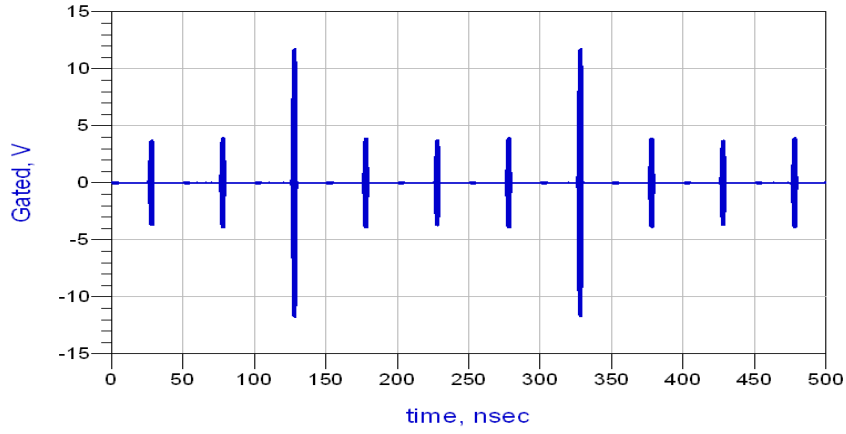

Figure 4.11: RF mixing stage simulation output [8]

However, in the implemented transmitter, actual test results were differed from the simulation results. Both simulation and implementation test results for pulse amplitude modulation stage were similar. But in the implemented transmitter, before mixing the baseband data pulses with 4.44 GHz carrier in the mixer stage, the ratio between "high" and "low" pulse was 3:1, which is acceptable. However, the ratio changes to an unacceptable level of approximately 2:1 after the carrier mixer. This ratio diminution is due to the fact that mixers are nonlinear by nature. A wideband mixer circuit is composed of nonlinear components like diodes, MOSFETs, multipliers and other CMOS elements. The ideal and real transient characteristics of these elements differ in great extent across the frequency bands. The ceramic surface mount mixer used for the up conversion of the baseband signal in DCSR transmitter is a wideband mixer (SIM-73L+, made by Mini Circuits), so the mixer's nonlinear characteristics very with frequency. Apart from nonlinearity, mixers also suffer from conversion losses, insertion losses and intermodulation distortions, which makes it difficult to model the overall loss of a wideband mixer and to predict the influence of it on the RF signal at the output of mixer accurately.

The output of the implemented transmitter before antenna is shown in the Figure 4.12. We can clearly see that the amplitude ratio between high and low pulses is 2.15:1. It should be noted that, regardless of the actual amplitudes of the pulses, the ratio is almost the same at RF mixer stage also.

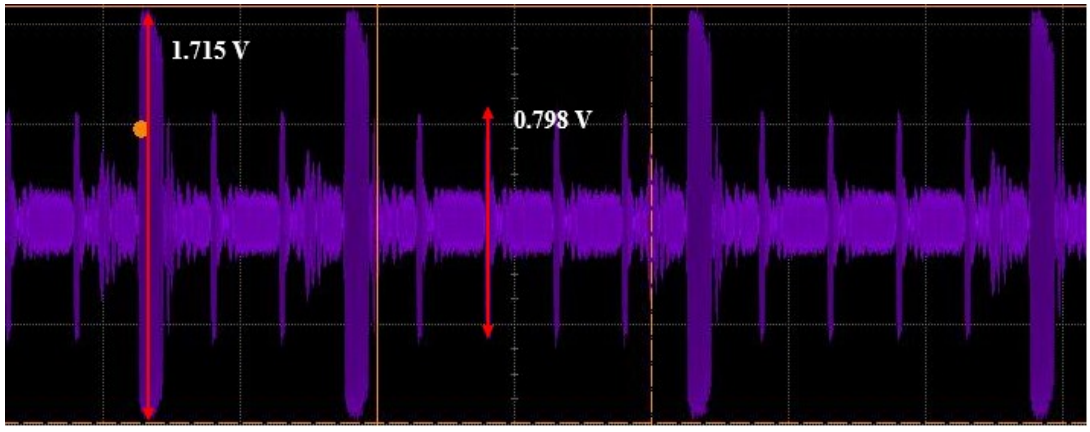

Figure 4.12: Pulse ratio at the output of DCSR transmitter

4.4 Circuit Level Modifications to Overcome Mixer Nonlinearity

The function of DCSR IR UWB receiver is based on the envelope energy detection technique. The received signal at the receiver is squared and energy of the squared signal is used for decision making and the original data extraction. Therefore, for the DCSR decoding algorithms to function properly in the receiver without any performance degradation, it is necessary to achieve minimal pulse ratio of 3:1 between high and low pulses at the transmitter output.

While having a pulse ratio greater than 3:1 is acceptable, but too large ratio might result in inaccurate performance and cause deviations in the actual bit error rate test results. Thus, 3:1 ratio should be selected as ideal while measuring the bit error rate performance of the system. To obtain the required ratio and to conduct bit error rate tests, the gain of each Op Amp in the PAM stage is modified for the moment, according to equation 4.1.

The gain of the Op Amp 2 was reduced to 2.161 from 3, using the resistors R_1=805 Ω and R_2 =1.74 kΩ. The gain was reduced instead of increasing it because, (a) increasing the Op Amp gain using R_2 > 3 kΩ results in a V_{out} level which exceeds the saturation voltage level of the RF mixer circuit, (b) decreasing only R_1 increases the V_{out} and (c) using any value of R_2 above 1.9 kΩ to increase the gain resulted in dramatic increase of pulse overshooting

and pulse expansion phenomenon (pulses were expanded beyond 6.5 ns) at the output of Op Amp 2. Pulse overshooting not only increases the circuit level noises, but also increases the ringing effect (an unwanted oscillation) in the DCSR signal. Pulse expansion reduces the bandwidth of the UWB signal and changes the spectral characteristics in frequency domain. And to compensate the loss of gain in Op Amp 2, the gain of Op Amp 1 was reduced to 0.23 using R_1=2.35 kΩ and R_2=550 Ω. In summary, modified gains are:

$$\text{Op Amp 2} = (1.74/0.805) = 2.161$$

$$\text{Op Amp 1} = (0.550/2.35) = 0.23$$

Therefore, the gain ratio (also the pulse ratio) between the Op Amps is increased from 3:1 to 9.4:1 at the pulse amplitude modulation stage. Obtained simulation results of the modified pulse amplitude modulation stage circuits are provided in Figure 4.13. The output of the pulse combiner after the modifications in the Op Amp gains can be seen in the Figure 4.14.

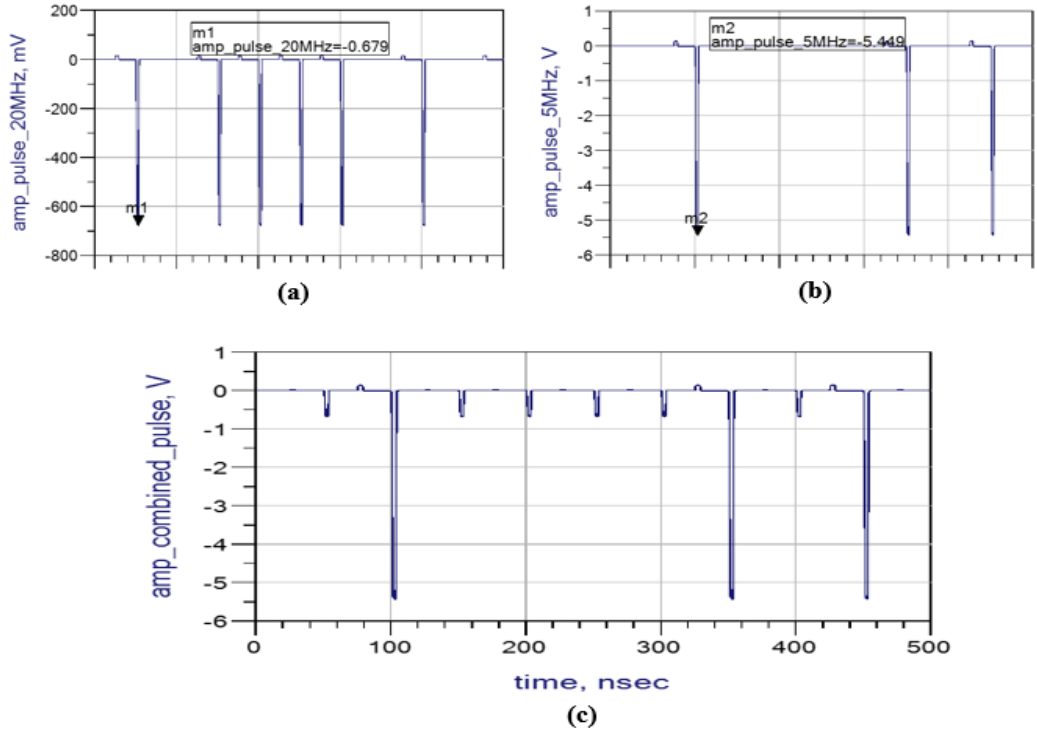

Figure 4.13: ADS simulation results for (a) output of Op Amp 1, (b) output of Op Amp 2 and (c) pulse combiner output

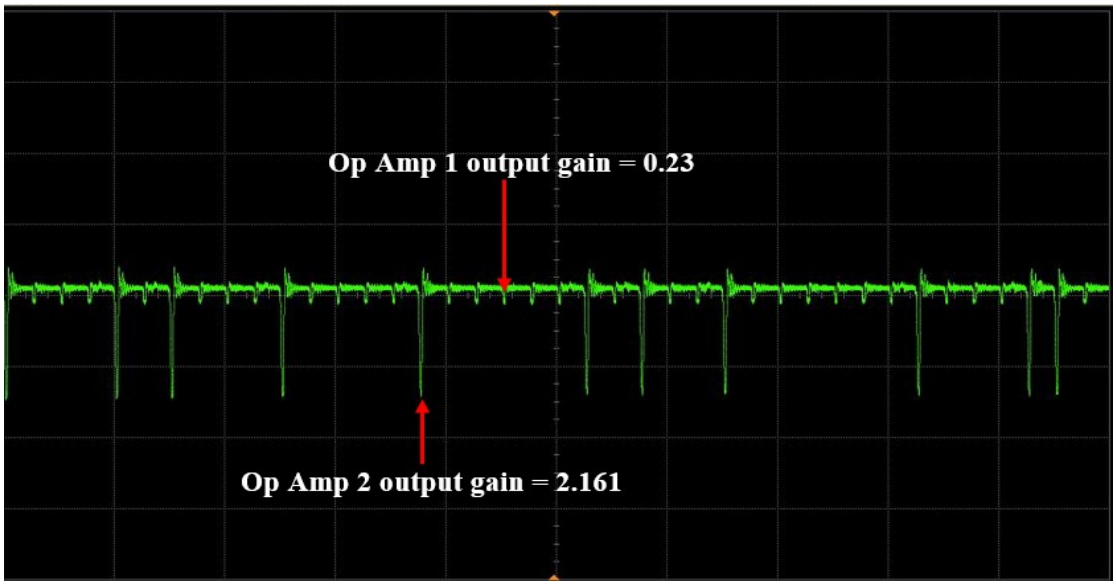

Figure 4.14: Modified pulse amplitude modulation stage output

After the gain modifications of the Op Amps at pulse amplitude modulation stage, the pulse ratio between high and low pulses became 3.0016:1 at the output of RF mixer, as shown in the Figure 4.15.

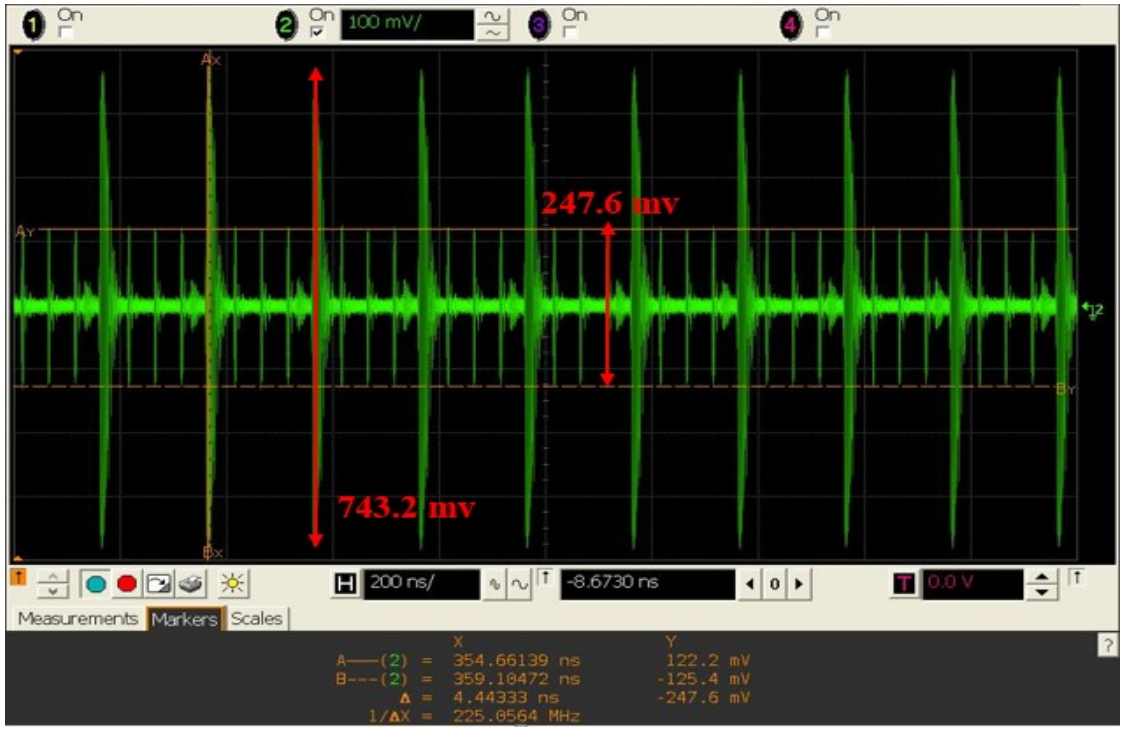

Figure 4.15: Desired pulse ratio after RF mixer stage

While changing the gains of Op Amps, only the amplitude ratio between high and low pulses were considered, not the energy in those pulses or the actual amplitude levels of the pulses at pulse amplitude modulation stage output. This is because, once the required pulse ratio of 3:1 is obtained after RF mixer stage, power spectrum of the DCSR UWB can be modified uniformly using attenuation or amplification, in order to keep the signal radiated by the antenna within the maximum EIRP emission level permitted by FCC.

Before radiating using the antenna, DCSR signal with desired pulse ratio is passed through spectral emission controllers- a pulse polarity modulator, band pass filter and a high power amplifier, to meet the commercial UWB spectral emission requirements defined by FCC.

The power amplifier used before transmitting the signal to antenna is MWT 6Y341. A minimum signal power attenuation of 12 dB is needed before the power amplifier in order to maintain the desired pulse ratio at the output of transmitter. This attenuation is required because the amplitude of high pulse is too large for the power amplifier and reaches saturation level. Also, it should be noted that an attenuation greater than 21 dB is required to keep the DCSR spectrum under FCC UWB spectral mask. So an attenuator was placed after RF mixer. Transmitter (power amplifier) output after 15 dB attenuation is provided in the Figure 4.16, where the high pulses have the amplitude of 3.613 V and low pulses have an amplitude of 1.198 mV. Therefore, the ratio is 3.015:1, in this case (carrier signal power was kept at 351.14 mV).

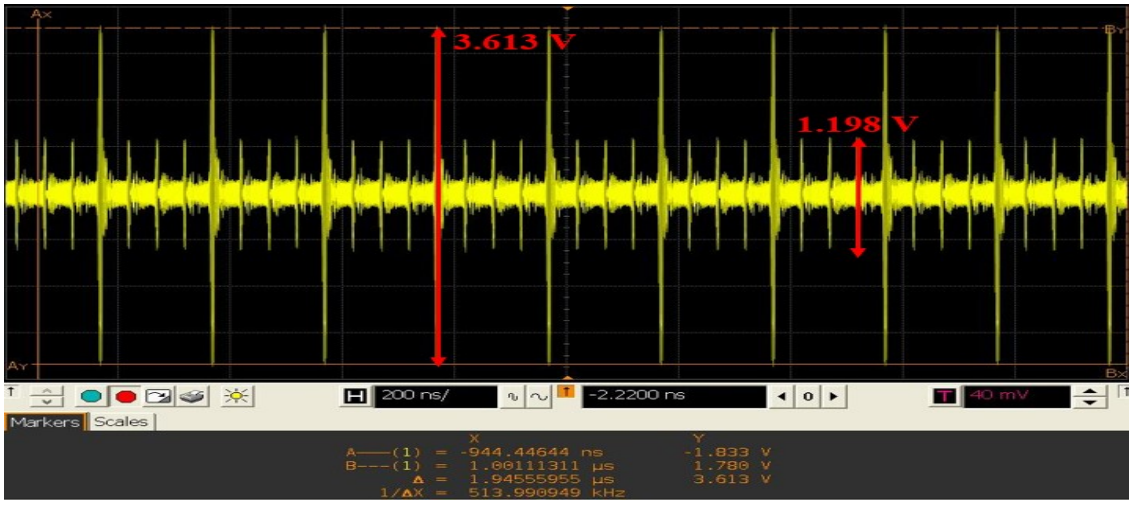

Figure 4.16: Output of DCSR transmitter before antenna

CHAPTER 5 THE PROPOSED TRANSMITTER TEST SEQUENCE GENERATION AND BIT ERROR RATE TESTS

This chapter proposes a new way of transmitter test sequence generation and presents the conducted bit error rate test procedures and results of the DCSR IR UWB transceiver. Bit error rate measurements were conducted in both ideal wireless testing environment in the absence of multipath and in the standard laboratory environment. Results are tabulated and analyzed.

5.1 Existing Data Bit Generation in DCSR Transmitter

During the tests, since the MAC layer is not yet developed for the current DCSR UWB system, the data is given in the form of a binary data bit sequence. The data bit sequence is digitally generated in [7] by using a linear feedback shift register. The length of the shift register is N=4, therefore it generates 2^N-1=15 bits in a sequence. The data bit sequence generated is "110001001101011" and the sequence repeats in cyclic order. The linear feedback shift register generates the bit sequence using a transmitter clock implemented in FPGA [7].

The number of bits which can be transmitted simultaneously in the DCSR UWB system at the moment is 2 (M=2, because N_f=4). A serial to parallel converter is used in [7] to convert the data bit sequence in serial format to 2 bit parallel format. After the parallel conversion, serial to parallel converter transmits two consecutive bits in the serial test sequence simultaneously using 10 MHz clock. For example, first two bits of the data bit sequence b_1=1 and b_2=1, are transmitted simultaneously as "11". So the two same data bit sequences (repeating sequence) of length equal to 15 can be arranged as,

"11 00 01 00 11 01 01 11 10 00 10 01 10 10 11" (5.1)

When the simultaneous bits "11" of the data bit sequence undergo DCSR modulation, they become data modulated pulses of "3111" (please see table 3.3). Digitally implemented

DCSR encoding algorithm (using VHDL) works in transmitter FPGA and uses 20 MHz clock [7]. Therefore, the DCSR data modulated clocks used for the generation of pulses have the frequency of 20 MHz. When the entire data bit sequence of equation 5.1 undergoes DCSR modulation, it becomes the data modulated pulse sequence of,

"3111 1311 1113 1311 3111 1113 1113 3111 1131 1311 1131 1113 1131 1131 3111" (5.2)

Simulations of the generation of DCSR data modulated clocks using the serial data bit sequence were done originally by [7]. Updated simulation results are provided in the Figure 5.1 and Figure 5.2. In the Figure 5.1, simulation result from 0 ns to 3600 ns, corresponding to two cycles of the data sequence, before the parallel conversion is shown. Signal "rst" represents reset function (active high reset of '1'). "clk" is the master clock of 40 MHz, generated by transmitter FPGA. "internal_data" is the repeating serial binary data bit sequence. "gain2" is the clock of the DCSR data modulated high pulse sequence (pulse 3) and "gain1" is the clock of DCSR data modulated low pulse sequence (pulse 1). (Please note that there is a delay in the conversion of data sequence bits to their corresponding DCSR data modulated pulses).

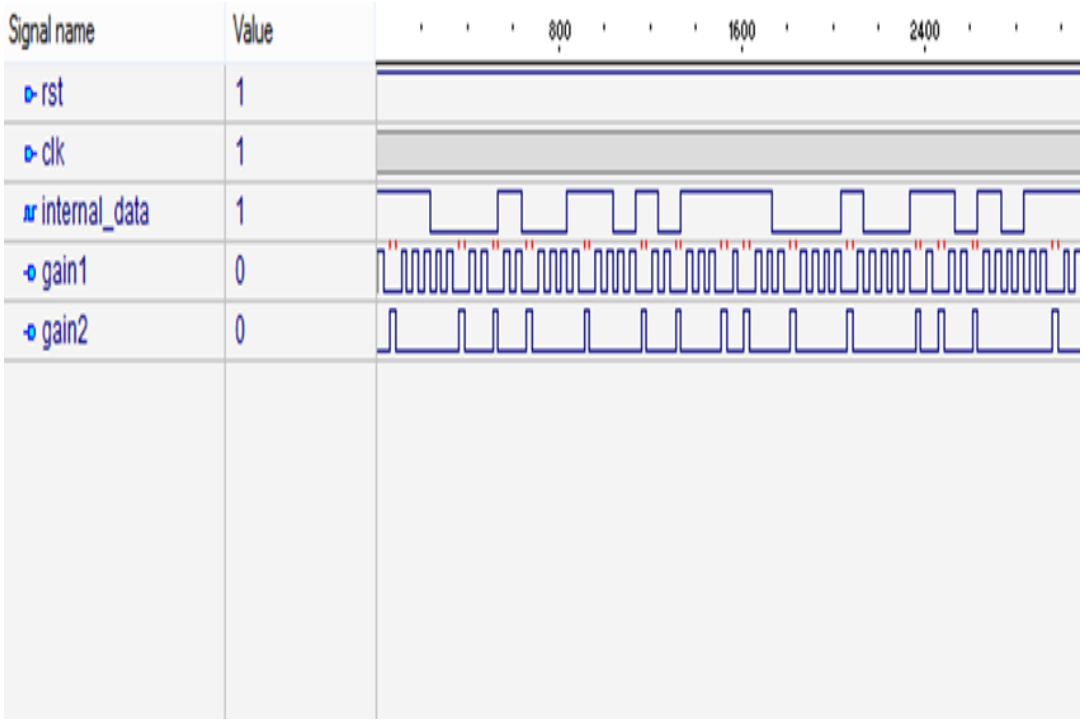

Figure 5.1: DCSR encoding simulations: Corresponding to data bit sequence

Simulation result from 4800 ns to 8000 ns, corresponding to the generation of DCSR data modulated pulses using the data bit sequence given in the equation 5.1, is shown in the Figure 5.2 [7]. “clk_20M” and “internal_clk10M” are the clocks used for the DCSR pulse generation and serial to parallel conversion respectively.

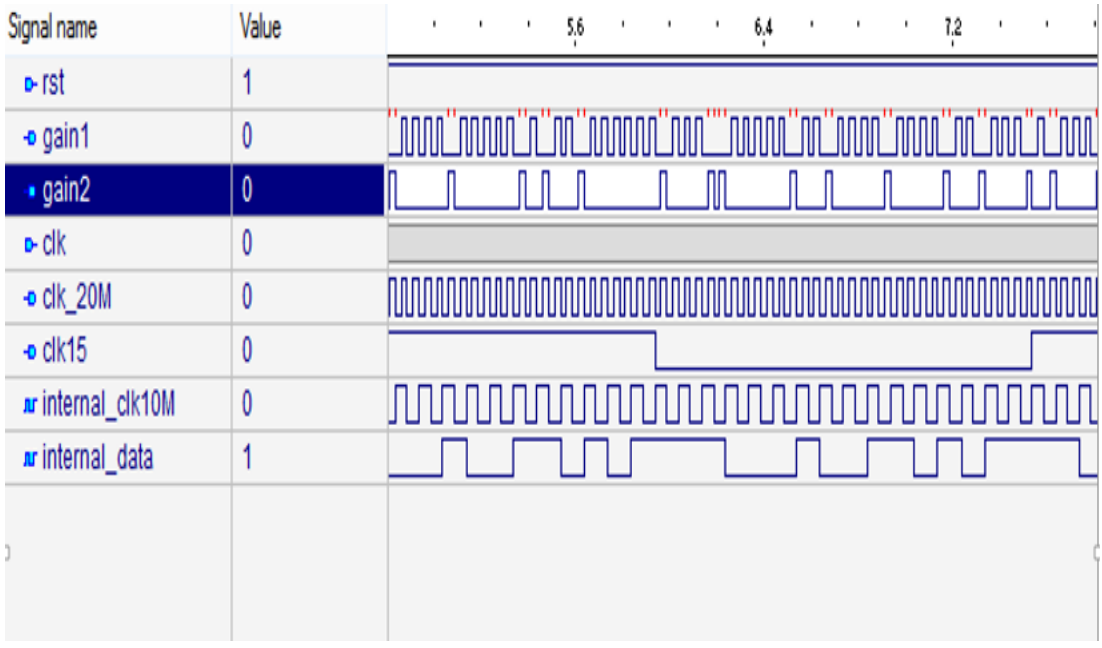

Figure 5.2: DCSR encoding simulations: Corresponding to pulse generation

5.2 Bit Error Rate Tester

A bit error rate tester (BERT) is necessary to measure the bit error rate performance of a communication system. Bit error rate (BER) performance of DCSR UWB transceiver was measured using Tektronix Packet BERT ™ 200 [38]. This is a general purpose BERT that can measure BER performance of any communication system from DC to 200 MBPS. Apart from BER measurement of binary data sequence, it’s also possible to generate packetized data sequence as well, and the BER of data packets can be measured using this BERT. Two main modules in the BERT are ‘generator’ and ‘analyzer’, as shown in the Figure 5.3.

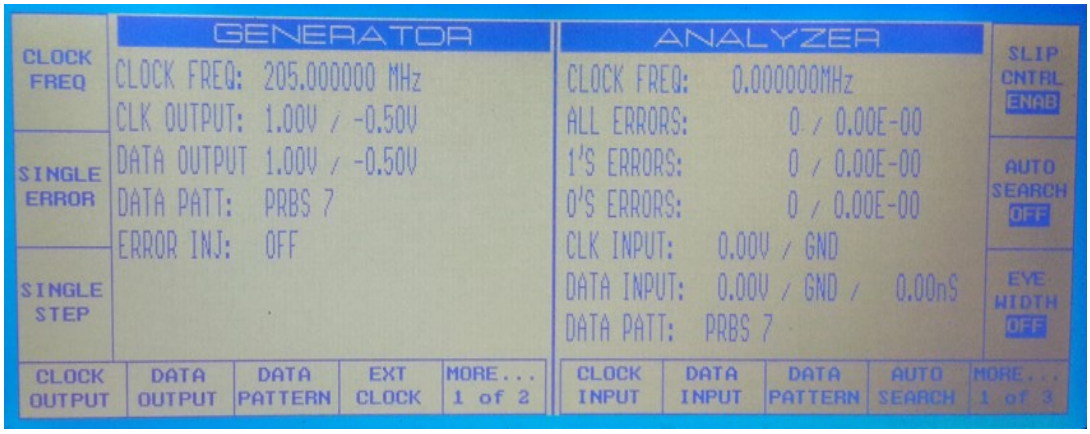

Figure 5.3: 'generator' and 'analyzer' of BERT

Generator: Test data bits are generated using the 'generator' of BERT and sent to DCSR transmitter, where they undergo DCSR modulation. 'Generator' offers different types of data sequence generation modes like pseudo random bit sequence (PRBS), word (decimal and ASCII) and mixed formats. Each bit's properties like amplitude, duration, threshold voltage, polarity and the delay are defined in the 'generator'. Two separate data sequences can be generated and transmitted simultaneously using two available data output ports (only one data port was used while conducting our BER tests).

Analyzer: Extracted test bit sequences from DCSR receiver is sent to 'analyzer'. In the 'analyzer' the received data bits are compared with transmitted data bits for the bit error rate analysis of the system.

BER analysis occurs only if the transmitter is synchronized with the receiver. Two separate clocks generated from the transmitter and receiver are given to 'generator' and 'analyzer' of BERT respectively, as external clocks. These verify the synchronization between transmitter and receiver before the analysis of data bits for BER measurement.

5.3 Test Sequence Generation for Bit Error Rate Tests

To conduct the bit error rate performance tests of implemented DCSR UWB transceiver, the linear feedback shift register (LFSR) described in the section 5.1 of this chapter, which

was used to generate binary data bit sequence was removed from the DCSR transmitter implementation. Therefore, with the absence of digitally implemented data bit generator, the DCSR data modulated pulses were created by DCSR encoding module using the test data bit stream which was generated directly by the BERT. Test sequence from BERT was given as external data signal to DCSR encoding block, using a port of transmitter FPGA.

With no test sequences (from "internal_data") during the simulations, "0000..." was provided as the incoming data sequence from the bit error rate tester to verify the updated transmitter DCSR encoding module. When a stream of 0s from an input port ("data_in") is used as data bits, the continuous DCSR encoded pulse sequence generated is "1311 1311..." as shown in the Figure 5.4. 1311 are the DCSR data modulated pulses of bits 00.

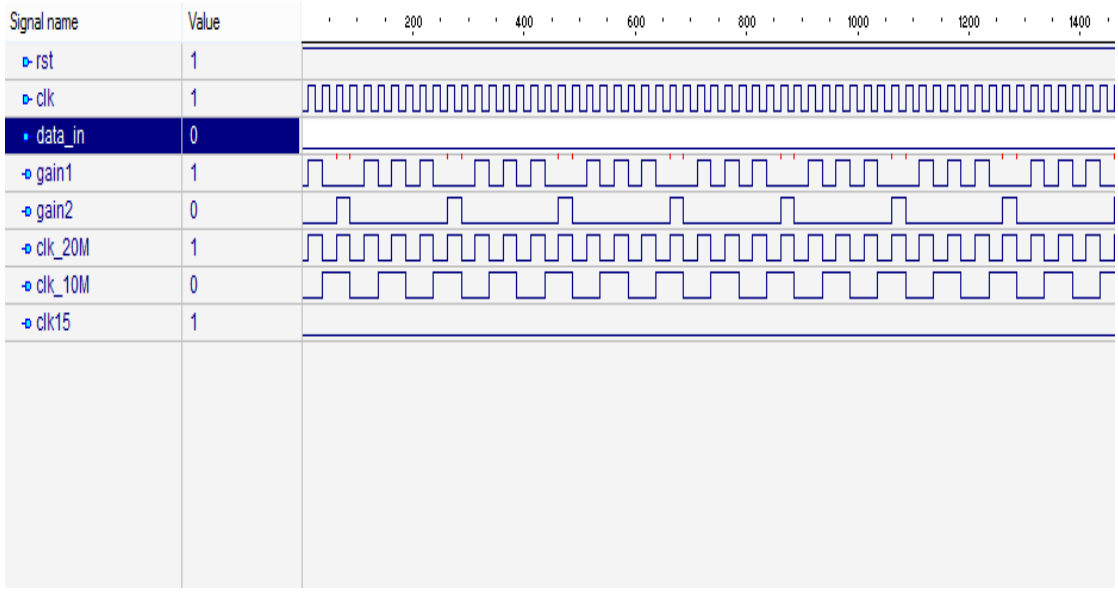

Figure 5.4: DCSR data modulation when bits b=0

Generation of bit sequence using BERT: It should be noted that the same test bits "110001001101011" are generated using the bit error rate tester, however, the bits in the test sequence were arranged as "111100010011010"- the last two bits of the original sequence were moved to the beginning of the sequence. The last two "11" bits were placed at the start because, this bit arrangement makes it easier to distinguish the separation point between two consecutive test sequences, when the same test sequence repeats cyclically while running the bit error rate tests.

The Packet BERT 200 used for BER tests provides different options to generate the test bit sequence. Pseudo random binary sequence (PRBS) mode can be used for the generation of random binary bits. PRBS mode can generate the random sequences of lengths up to 2^{31}-1, using shift registers. However, to generate customized test sequences, BERT has the option to load the input for the generation of binary data bit sequences in regular 'word' format, using an external storage device (floppy disk). The maximum bit length of words permitted in 'word' format is 256 kilobits. Test bit sequence generation information can be provided using decimal number system or ASCII characters, if 'word' format is used.

To conduct BER tests, a fixed decimal number sequence of length 15 is used for the generation of binary test sequence in BERT. The decimal number sequence was loaded to BERT using 'word' format. In 'word' format, each word in the decimal sequence is separated by space (for example, '235' is a word). The decimal number sequence used is:

35 235 145 245 200 122 100 61 178 30 89 143 172 71 214 (5.3)

Default resolution length for each word is 8 bits in the BERT. If the word length is 15, total number of bits created is 15 X 8 = 120 (total bit length). Decimal word sequence to binary test data sequence conversion, which occurs in the BERT is given in the Table 5.1.

Decimal word	b_7	b_6	b_5	b_4	b_3	b_2	b_1	b_0
35	0	0	1	0	0	0	1	**1**
235	1	1	1	0	1	0	1	**1**
145	1	0	0	1	0	0	0	**1**
245	1	1	1	1	0	1	0	**1**

Decimal word	b_7	b_6	b_5	b_4	b_3	b_2	b_1	b_0
200	1	1	0	0	1	0	0	**0**
122	0	1	1	1	1	0	1	**0**
100	0	1	1	0	0	1	0	**0**
61	0	0	1	1	1	1	0	**1**
178	1	0	1	1	0	0	1	**0**
30	0	0	0	1	1	1	1	**0**
89	0	1	0	1	1	0	0	**1**
143	1	0	0	0	1	1	1	**1**
172	1	0	1	0	1	1	0	**0**
71	0	1	0	0	0	1	1	**1**
214	1	1	0	1	0	1	1	**0**

Table 5.1: Binary test sequence generation from 'word' format in BERT

The generated serial binary test bit sequence repeats itself in cyclic order. A binary bit from each word in the word test sequence is transmitted at a time sequentially using the

data output port. As there are two data sequence output ports in BERT 'generator', two generated test sequences can be transmitted simultaneously. However, during the BER tests of DCSR system, only one test sequence was generated and transmitted using one output port. The BERT offers flexibility during test sequence bits selection, using the serial transmission mode - i.e., the serial transmission mode can be chosen as either least significant bit (LSB) first (b_0) or the most significant bit (MSB) first (b_7). In our testing cases, LSB mode was chosen and the bits b_0 of every word in the decimal sequence are transmitted in each cycle at the rate of 10 MHz. Since LSBs are transmitted, the incoming test bit sequence from BERT to transmitter FPGA is "111100010011010", as shown in the Figure 5.5.

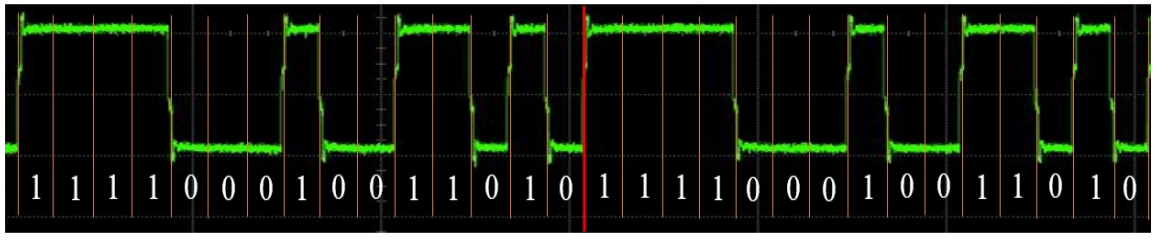

Figure 5.5: Generated test data sequence by BERT (2 cycles)

Only the payload was generated in test sequence, without the generation of preamble, overhead or delay. This was done for two main reasons. First reason- it was possible to keep them as optional entities while generating the payload in the BERT and second- the packet based data sequence detection techniques come under top layers, not in physical layer. Any layers other than the physical layer are not developed for DCSR system yet.

A clock of 10 MHz is generated in DCSR transmitter FPGA and is given to the 'generator' of BERT as external clock signal, using an output port in FPGA. External clock is used as the master clock for 'generator' and serves the purposes of the generation of test bit sequences and the verification of synchronization between transmitter and receiver (or 'generator' and 'analyzer').

Original data sequence is extracted at the receiver from DCSR data modulated pulses according to the DCSR decoding method mentioned in [4], which uses direct searching code synchronization algorithm, as mentioned in [37]. The simultaneous data bits $\widehat{b}_1$ and $\widehat{b}_2$

are extracted as two separate sequences in [7] (please refer Figure 3.9). The extracted parallel data bit sequences are converted to a serial data sequence using a 2 to1 parallel to serial converter implemented in receiver FPGA by [12]. The parallel to serial conversion is done at 10 MHz. The converted serial data sequence is taken as the output from receiver FPGA using a port and is given to 'analyzer' of BERT for BER analysis of the DCSR system. The generated and received serial data bit sequence trains at the 'generator' and 'analyzer' of the BERT are shown in the Figure 5.6.

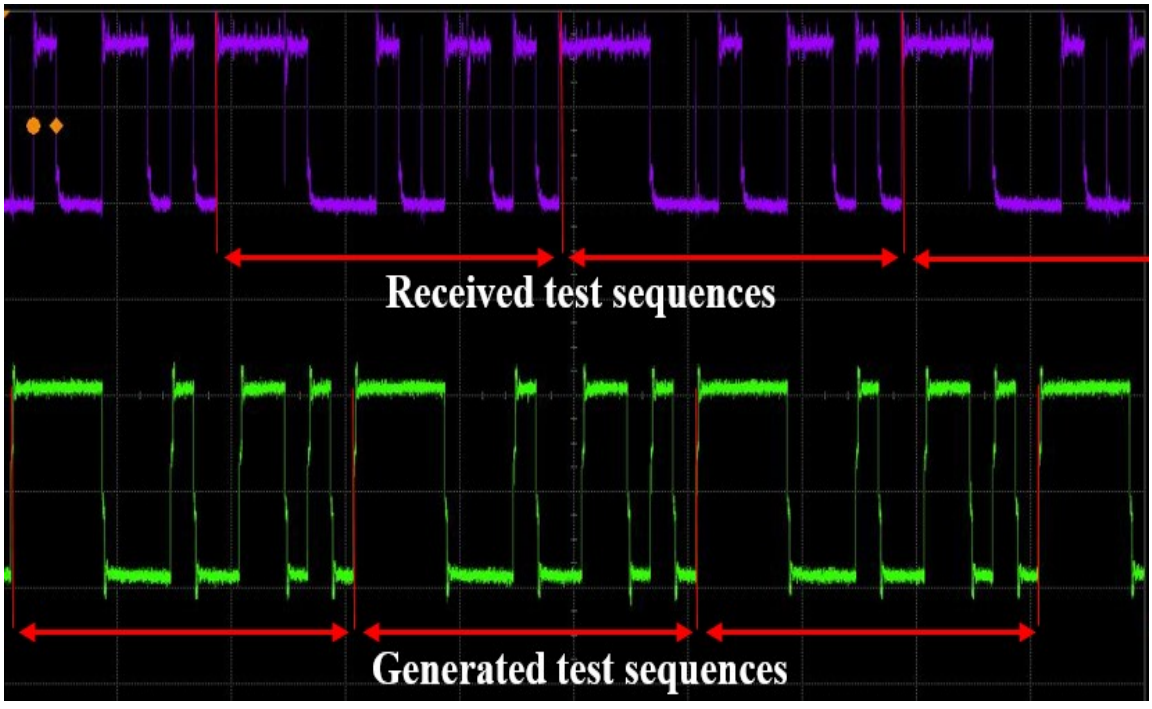

Figure 5.6: Test data sequences at 'generator' and 'analyzer' of BERT

Each bit in the received data sequence is compared with the original transmitted bit in the 'analyzer' in order to find the bit error rate. 'Analyzer' operates using 10 MHz master clock, which is generated in receiver FPGA. Additionally, the clock should be synchronized with 'generator' clock to confirm the synchronization between transmitter and receiver.

5.4 Bit Error Rate Tests in Practical Environments

The main aim of the conducted BER tests is to validate the feasibility of the implemented DCSR transceiver in the wireless channel environment. So the BER tests were conducted using two channel conditions, a) in an ideal indoor LOS channel with no multipath components - using an anechoic chamber and (b) in an indoor LOS multipath channel, identical to the channel 7 of IEEE 802.15.4a channel model (please refer Table 2.3) - using a standard microwave/RF laboratory environment. BER performance of the system was compared with reference to the distance between transmitter and receiver antennas in both the test environments, not with respect to SNR. To compare the BER performance of DCSR modulation scheme with the simulation results obtained in [6], the tests need to be conducted with respect to SNR (E_b/N_o). Figure 5.7 shows the block diagram of bit error rate test set up for the DCSR transceiver.

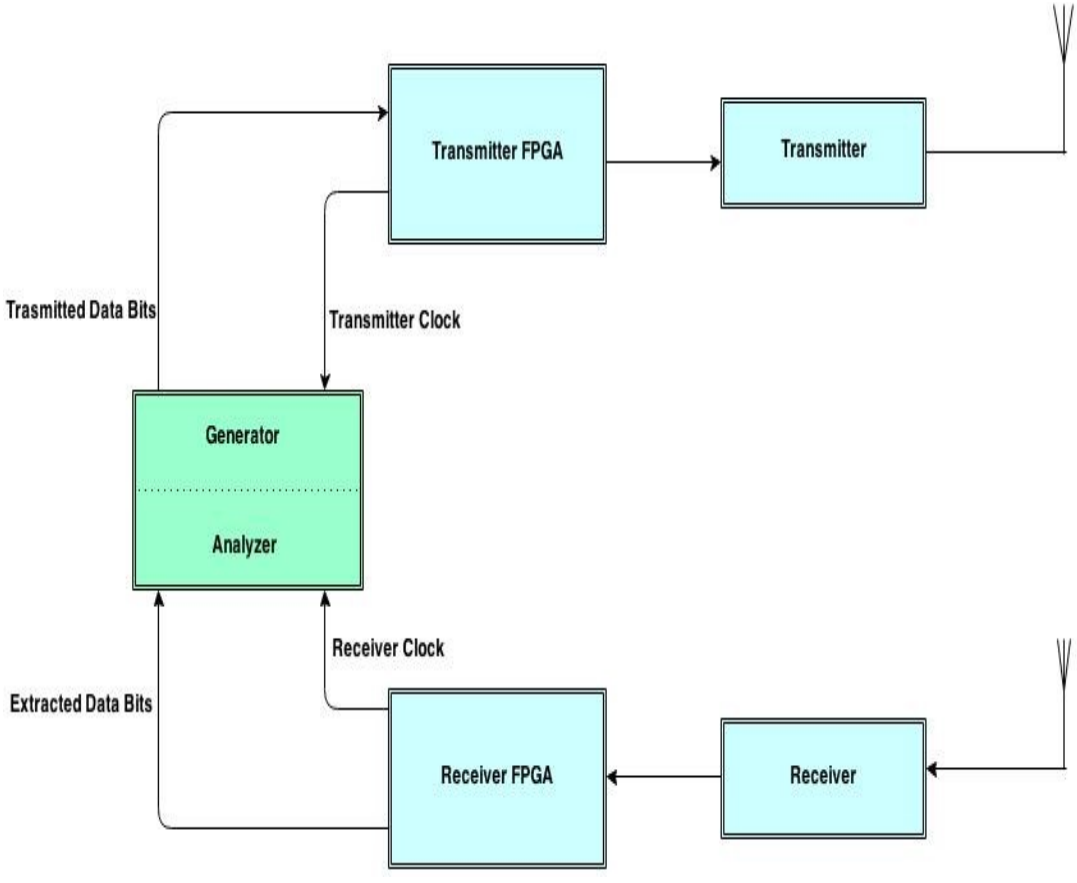

Figure 5.7: BER test setup of DCSR transceiver

Before moving to the actual tests on the transceiver using wireless communication channels, the BER test was conducted using wired connection between transmitter and receiver in order to verify the basic operational principle of the developed physical layer of DCSR system. No bit error was existed (BER = 0 X 10^{-8}), which demonstrates the functioning capability of both transmitter and receiver. It also proves the effectiveness of DCSR modulation and demodulation algorithms.

Two identical ultra-wideband planar elliptical dipole antennas were used at the end of transmitter and receiver during the BER tests of the system using wireless communication channels. The used PulsON 400 UWB antennas were developed by Time Domain Inc. [39]. In both the ideal and multipath wireless channel BER test scenarios, the antennas were placed in such a way that the LOS signal propagation was possible between them.

The antennas were faced each other using their peak radiation direction (main lobe - 0^0 azimuth plane at 4.44 GHz). Beam patterns of the used antennas can be found in [39]. Height between both the antennas was kept same from the ground level in both testing cases (no elevation). Though FCC regulation requires maximum EIRP emission mask in all directions, most energy of the UWB spectrum is concentrated in the antenna's main lobe (peak radiation direction), making the energy in other directions (side lobes, if any) well below the maximum permitted EIRP level for commercial UWB.

5.4.1 BER Results in ideal LOS Environment

The first set of BER tests on the transceiver were done inside the anechoic chamber, in the absence of multipath propagation and interferences from other wireless communication devices. This wireless channel condition serves as an ideal channel with LOS propagation for BER measurements.

Since BER tests were conducted with respect to the distance between transmitter and receiver antennas, various measurements were recorded at the distances ranging from 0.05

meters to 2.5 meters. The tests were limited to approximately 2.5 meters, since that is the maximum possible testing distance inside our anechoic chamber. In all the tested cases, signal recovery unit functioned relatively well at the receiver, compensating for any losses or gains in the power level of the received signal. Since the operational principles of the system was already verified, the BER performance of the transceiver was in accordance with the predictions. Moreover, due to the absence of multipath and interferences, system performance was extremely reliable in all the tested cases, regardless of the distance. BER was very low**,** even at the maximum possible distance, as shown in the Figure 5.8. The obtained results are tabulated in the Table 5.2.

Distance between Antennas in meters	**BER Performance**
<0.05	0×10^{-8}
0.25	0×10^{-8}
0.5	0×10^{-8}
1	0×10^{-8}
1.5	0×10^{-8}
1.92	1.8×10^{-8}
2.5 (maximum possible distance)	4.15×10^{-6}

Table 5.2: BER test results in ideal LOS environment

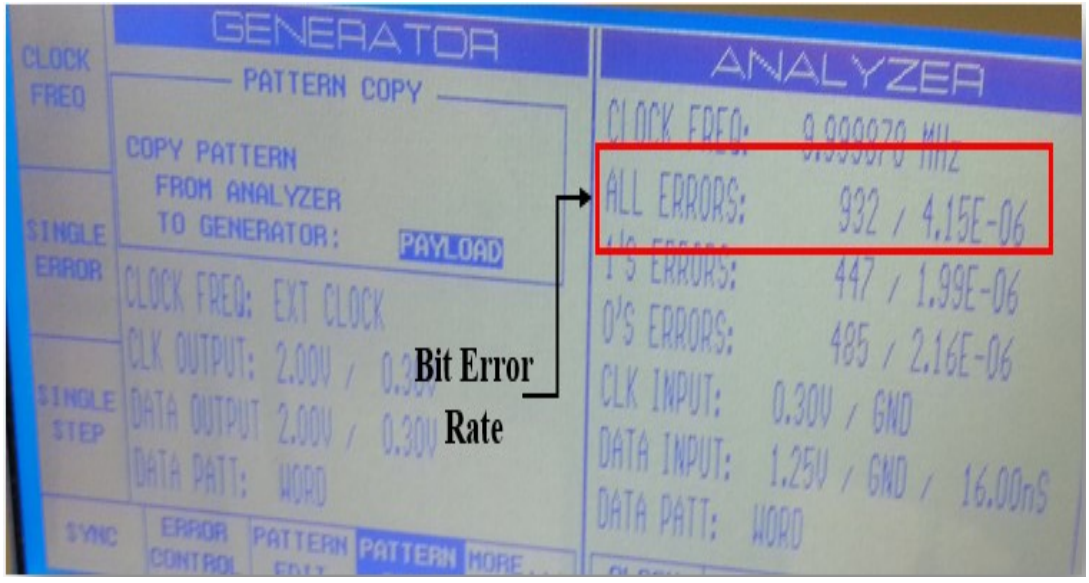

Figure 5.8: BER inside anechoic chamber when distance between antennas is 2.5 meters

5.4.2 BER Results in Multipath LOS Environment

After the verification of its performance in the ideal LOS channel condition using an anechoic chamber, the system was later tested using the standard RF and wireless communication laboratory LOS environment. This indoor channel's condition is similar to the multipath channel 7's environment of IEEE 802.15.4a channel model.

Like in the anechoic chamber, the measurements in this case were also taken by varying the distance between the antennas. Even when the antennas were very close to each other and the signal strength was good, bit errors began to appear during the test. However, unlike in ideal LOS channel environment, the received DCSR signal strength in this environment began to decline rapidly with reference to distance. Therefore, the synchronization between transmitter and the receiver was lost when the antennas were about 4.6 meters away from each other. After this distance, AGC at the signal recovery stage of the receiver was unable to recover the strength of the received signal.

Even when the AGC was able to recover the signal, bit error rates were varied due to the presence of the interferences and multipath propagation of UWB signal components. The multipath errors were caused because of the NLOS propagation of some IR signal components and these signal components were reflected back to receiver from obstacles like floor, wall and other lab equipments. The main interference came from the OFDM signal of 802.11a (WLAN), which operates using the frequency bands between 5.180 – 5.825 GHz. As wideband BPF used at the receiver's signal recovery stage doesn't has the sharp cut off frequency at 4.7 GHz, the interfering signal from the WLAN was not filtered out completely.

Multipath propagation and interference factors contributed to the uneven variations in bit error rates, even when the signal recovery stage was working properly. The obtained BER test results are provided in the Table 5.3. Obtained test results at every 1 meter interval are shown in the Figure 5.9.

Distance between Antennas in meters	**BER Performance**
<0.05	6.85×10^{-7}
0.25	8.43×10^{-5}
0.5	1.06×10^{-4}
1	1.25×10^{-4}
1.5	3.64×10^{-3}
2	8.74×10^{-3}

Distance between Antennas in meters	BER Performance
2.5	$6.71 X10^{-3}$
3	$1.13 X 10^{-2}$
3.5	$5.21 X 10^{-2}$
4	$5.61 X 10^{-2}$
4.4	$1.5 X 10^{-1}$
4.6	$4.98 X 10^{-1}$ (Sync lost)

Table 5.3: BER test results from multipath LOS environment

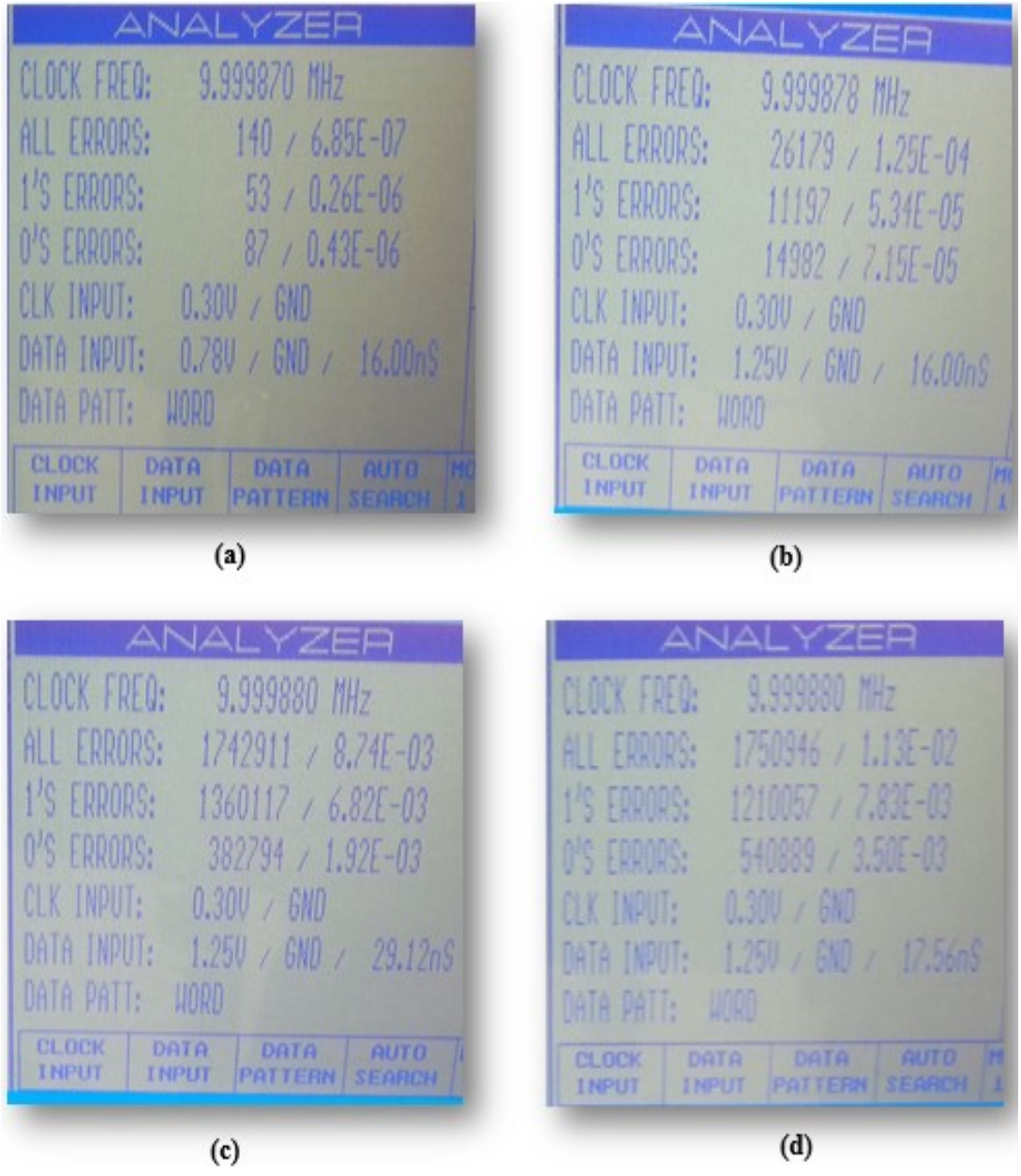

Figure 5.9: BER results in multipath LOS environment when antennas distance is: (a) 0.05 meter; (b) 1 meter; (c) 2 meters and (d) 3 meters

Finally, the obtained BER test results from both ideal indoor LOS communication channel environment of the anechoic chamber and the multipath indoor LOS communication channel environment of the RF/Microwave laboratory are compared using the graph in the Figure 5.10.

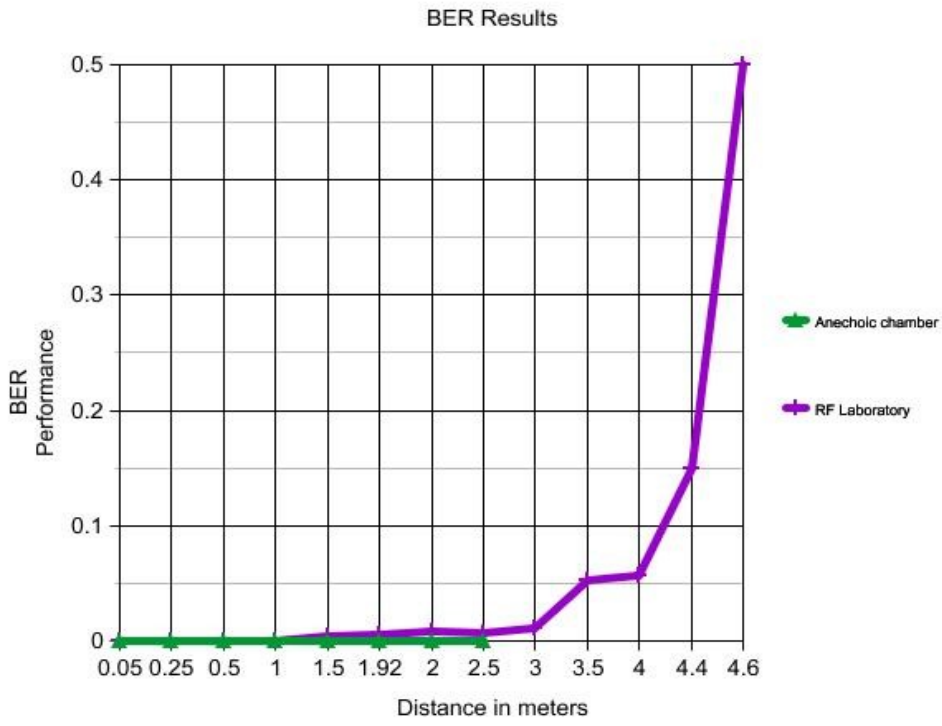

Figure 5.10: BER result assessments: Ideal and Multipath LOS Environments

CHAPTER 6 CONCLUSION AND FUTURE WORK

6.1 Conclusion

This thesis presented the recently conducted bit error rate assessment results of the newly developed prototype DCSR IR UWB transceiver. To measure the actual bit error rate performance of the transceiver, the issue of nonlinearity in the transmitter was addressed by achieving the desired DCSR pulse ratio at the transmitter output. To facilitate bit error rate tests, the existing digital binary data bit generation module in the transmitter was replaced with externally generated test sequences. The DCSR data modulated pulses were generated using these external test sequences in DCSR encoding module. Thesis also proposed a new method for test sequence generation using a bit error rate tester and used the method to generate test sequences for bit error rate tests.

Binary test bits were used to generate DCSR data modulated pulses at the transmitter and the pulses were transmitted using the wireless communication channel. The original test bits were extracted at the receiver from DCSR data modulated pulses using DCSR decoding algorithms. Recovered bits were compared with transmitted bits in a bit error rate tester for the performance analysis of the DCSR transceiver.

The bit error rates were measured with respect to the distances between transmitter and receiver antennas using practical wireless environments. Bit error rate tests were conducted in two communication channel conditions. In ideal LOS channel condition, the transceiver performed extremely well with minimum errors. However, in non-ideal multipath LOS channel condition, the performance was reasonable, which agrees with theoretical predictions. Additionally, operating principles of the DCSR system were also verified by conducting the BER test using wired connection.

Results of the bit error rate tests have shown that the prototype DCSR transceiver meets the theoretical design requirements effectively.

6.2 Future Work

Transceiver, being the physical layer of the DCSR system, is still in its developmental stage. Some of the important works which are in need to be addressed in the near future can be summarised as:

- The digital modulation scheme combined with analog circuit elements results in significant circuit level noises at both transmitter and receiver, which couldn't be modeled or simulated. Effective noise reduction techniques should be investigated and implemented to eliminate them.

- The original data bits were extracted from the DCSR data modulated pulses using direct search code synchronization algorithm in the receiver. Simulation results have shown that there are two other algorithms which provide superior performances compared to direct search algorithm. Bit error rate analysis of the system by implementing those two algorithms at the receiver would be useful.

- Conducting BER tests based on SNR (E_b/N_0) levels is desirable in order to compare the efficiency of DCSR modulation scheme with other existing impulse radio modulation schemes.

- The newly implemented DC blocking circuit in the receiver consists of a potentiometer which causes slight variations in BER results every time. Hence, appropriate tuning of the circuit is required.

REFERENCES

[1] Federal Communications Commission, Revision of Part 15 of the Commission's Rules Regarding Ultra-wideband Transmission Systems: First Order and Report Tech. Report, FCC 02-48, April 2002.

[2] M. Ghavami, R. Kohno and L. Michael, "Ultra Wideband Signals and Systems in Communication Engineering", 2nd Edition, Wiley, 2007.

[3] H. Nie and Z. Chen, "Code-Shifted Reference Ultra-wideband (UWB) Radio," Proc. of Sixth Annual Conference on Communication Networks and Services Research (CNSR2008), pp. 385-389, May 2008.

[4] H. Nie and Z. Chen, "Differential Code-Shifted Reference Ultra-wideband (UWB) Radio," Proc. IEEE 68th Vehicular Technology Conf., pp. 1-5, September 2008.

[5] H. Nie and Z. Chen, "Performance Analysis of Code-Shifted Reference Ultra-Wideband (UWB) Radio," Proc. of IEEE Radio and Wireless Symposium, pp. 396-399, January 2009.

[6] H. Nie and Z. Chen, "Performance Evaluations for Differential Code-Shifted Reference Ultra-wideband (UWB) Radio," Proc. IEEE International Conf. Ultra-wideband, pp. 274-278, September 2009.

[7] C. Wei, "Baseband Transceiver for Code-shifted Reference Impulse-Radio Ultra-wideband (CSR IR-UWB) System," MASc thesis, Dalhousie University. Halifax, NS, 2010.

[8] J. Lowe, “RF Transceiver for Code-shifted Reference Impulse-Radio Ultra-wideband (CSR IR-UWB) System,” MASc thesis, Dalhousie University, Halifax, NS, 2010.

[9] A. Pearce, “Spectral Line Reduction in an RF Transceiver for Differential Code Shifted Reference for Ultra-wideband System,” M. Eng. Project, Dalhousie University, Halifax, NS, 2011.

[10] K. Aldubaikhy, “Differential Code-Shifted Reference Impulse-Radio Ultra-wideband Receiver: Timing Recovery and Digital Implementation,” MASc. thesis, Dalhousie University, Halifax, NS, 2012.

[11] T. Arabi, “Pulse Synchronization and Timing Recovery in Differential Code-Shifted Reference Impulse-Radio Ultra Wideband (DCSR IR-UWB) System,” MASc thesis, Dalhousie University, Halifax, NS, 2013.

[12] M. Liu, “Differential Code-Shifted Reference Impulse-Radio Ultra-wideband Receiver: Signal Strength Adjustment and Implementation”, MASc. thesis, Dalhousie University, Halifax, NS, 2014.

[13] I. Oppermann, M. Hamalainen, and J. Linatti, “UWB Theory and Applications”, John Wiley & Sons, 2004.

[14] IEEE 802 Part 15.3: “Wireless Medium Access Control (MAC) and Physical Layer (PHY) Specifications for Higher Rate Wireless Personal Area Networks (WPAN),” 2003.

[15] T. T. K. Tsang and M. N. El-Gamal, “Ultra-wideband (UWB) Communications Systems: An Overview”, Proc. of IEEE-NEWCAS Conf., pp. 381-386, January 2005.

[16] IEEE Std 802.15.4a, "Amendment to 802.15.4-2006: Wireless Medium Access Control (MAC) and Physical Layer (PHY) Specifications for Low-Rate Wireless Personal Area Networks (LR-WPANs)", 2007.

[17] M. Z Win, D. Dardari, A. F Molisch, W. Wiesbeck, and J. Zhang, "History and Applications of UWB," Proc. of the IEEE, vol. 97, no. 2, pp.198–204, February 2009.

[18] Z. Zou, "Impulse Radio UWB for the Internet-of-Things: A Study on UHF/UWB Hybrid Solution", Doctoral thesis, KTH Royal Institute of Technology, Stockholm, Sweden, 2011.

[19] H. Nikookar and R. Prasad, "Introduction to Ultra Wideband for Wireless Communications", Springer Science + Business Media, 2009.

[20] S. A. Ghorashi, B. Allen, M. Ghavami, and A. H. Aghvami, "An Overview of MB-UWB OFDM", Proc. of IEEE Seminar on Ultra Wideband Communications Technologies and System Design, pp. 107-110, Jul 2004.

[21] J. Ryckaert, M. Badaroglu, C. Desset, V. De Heyn, G. ven der Plas, P. Wambacq, B. van Poucke, and S. Donnay, "Carrier-based UWB Impulse Radio: Simplicity, Flexibility, and Pulser Implementation in 0.18-μmCMOS", IEEE International Conf. on Ultra-Wideband (ICUWB 2005), pp. 432–437, September 2005.

[22] W. Schaefer, "Understanding Impulse Bandwidth Specifications of EMI Receivers," Proc. IEEE International Symposium on Electromagnetic Compatibility, Vol. 2, pp. 958-961, August 1999.

[23] J. Reed, "An Introduction to Ultra Wideband Communication Systems", Prentice Hall, 2005.

[24] J. Zhang, T. Adhayapala and R. Kennedy, “Role of Pulses in Ultra Wideband Systems”, Proc. IEEE International Conf. Ultra-Wideband, pp. 565-570, September 2005.

[25] H. Kim and Y. Joo, “Fifth-Derivative Gaussian Pulse Generator for UWB System”, Proc. IEEE Radio Frequency Integrated Circuits (RFIC) Symposium, pp. 671-674, June 2005.

[26] A. Serres and J. Ewerton, “A New Simple UWB Monocycle Pulse Generator”, Proc. 13th IEEE International Conf. Electronics, Circuits and Systems, pp. 1212-1215, December 2006.

[27] J. Han and C. Nguyen, “A New Ultra-wideband, Ultra-short Monocycle Pulse Generator with Reduced Ringing”, IEEE Microwave and Wireless Components Letters, Vol.12, Issue 6, pp. 206-208, June 2002.

[28] J. Zhang, S. Zhang, S. Wang, J. Qiu and R. Zhou, “A Fully Integrated CMOS UWB Transmitter”, Proc. 7th International Conf. ASIC, pp. 373-374, October 2007.

[29] J. Fernandes, H. Goncalves, L. Oliveira and M. Silva, “A Pulse Generator for UWB-IR Based on a Relaxation Oscillator”, IEEE Transactions on Circuits and Systems II: Express Briefs, Vol. 55, Issue 3, pp. 239-243, March 2008.

[30] J. Zhao, C. Maxey, A. Narayanan and S. Raman, “CMOS Wideband Pulse Generators for UWB Transmitter Applications”, Proc. IEEE Sarnoff Symposium, pp. 1-4, March 2006.

[31] A. F Molisch, “Ultra-Wide-Band Propagation Channels,” Proc. of the IEEE, vol. 97 no. 2, pp. 353–371, February 2009.

[32] A. F. Molisch, K. Balakrishnan, C. Chong, S. Emami, A. Fort, J. Karedal, J. Kunisch, H. Schantz, U. Schuster and K. Siwiak, “IEEE 802.15.4a Channel Model - Final Report”, IEEE 802.15-04-0662-02-004a, 2005.

[33] F. Nekoogar, “Ultra Wideband Communications: Fundamentals and Applications”, Prentice Hall, 2006.

[34] D. Porcino and W. Hirt, “Ultra Wideband Radio Technology: Potential and Challenges Ahead”, IEEE Communications Magazine, Vol. 41, Issue 7, pp. 66 – 74, July 2003.

[35] J. Linnartz, "Analysis of a Rake Receiver," Wireless Communication, 1999. Online available:http://www.wirelesscommunication.nl/reference/chaptr05/cdma/rakeperf.htm. (July 2015).

[36] D. L. Goeckel and Q Zhang, “Slightly Frequency-Shifted Reference Ultra-Wideband (UWB) Radio”, IEEE Transactions on Communications, Vol. 55, Issue 3, pp. 508 – 519, March 2007.

[37] C. Wei, H. Nie and Z. Chen, "Non-Data-Aided Code Synchronization for the Code-Shifted Reference Ultra-Wideband (UWB) System," Eighth annual Communication Networks and Services Research Conference (CNSR), pp. 56-60, May 2010.

[38] Manual, “Packet BERT 200 DC-200 Mb/s Bit Error Rate Tester”, Tektronix Inc.

[39] Datasheet, “PulseOn 400 Broadspec UWB Antenna”, Time Domain Inc.

[40] B. Sahukar, H. Nie & Z. Chen, “A Proposal for New Millimeter Wave Wideband Transceiver System – The Code Shifted Reference Impulse Radio System”, 2015 Global Symposium on Millimeter Waves, May 2015.

[41] B. Sahukar, H. Nie & Z. Chen, “Progress in Development of Differential Code Shift Reference Impulse Radio Ultra-Wideband Transceiver”, 2015 IEEE International Conference on Ubiquitous Wireless Broadband, October 2015.